University, Yonezawa, Yamagata 992, Japan.
(2) Ito, H.; Willson, C. G. *Polym. Eng. Sci.* **1983**, *23*, 1012.
(3) Ito, H.; Willson, C. G. In *Polymers in Electronics*; Davidson, T., Ed.; ACS Symposium Series 242; American Chemical Society: Washington, DC, 1984; p 11.
(4) MacDonald, S. A.; Ito, H.; Willson, C. G. *Microelectron. Eng.* **1983**, *1*, 269.
(5) Ito, H.; Willson, C. G.; Frechet, J. M. J. *Proc. SPIE—Int. Soc. Opt. Eng.* **1987**, *771*, 24.
(6) Grant, D. H.; Grassie, N. *Polymer* **1960**, *1*, 125.
(7) Matsuzaki, K.; Okamoto, T.; Ishida, A.; Sobue, H. *J. Polym. Sci., Part A* **1964**, *2*, 1105.
(8) Geuskens, G.; Hellinckx, E.; David, C. *Eur. Polym. J.* **1971**, *7*, 561.
(9) Lai, J. H. *Macromolecules* **1984**, *17*, 1010.
(10) Hatada, K.; Kitayama, T.; Okamoto, Y.; Yuki, H.; Aritome, H.; Namba, S.; Nate, K.; Inoue, T.; Yokono, H. In *Materials for Microlithography*; Thompson, L. F., Willson, C. G., Frechet, J. M. J., Eds.; ACS Symposium Series 266; American Chemical Society: Washington, DC, 1984; p 399.
(11) Crivello, J. V.; Lam, J. H. W. *J. Polym. Sci., Polym. Chem. Ed.* **1980**, *18*, 2697.
(12) Yuki, H.; Ohta, K.; Ono, K.; Murahashi, S. *J. Polym. Sci. Polym. Chem. Ed.* **1968**, *6*, 829.
(13) Yuki, H.; Ohta, K.; Hatada, K.; Okamoto, Y. *Polymer J. (Tokyo)* **1977**, *9*, 511.
(14) van Volkenburgh, R.; Greenlee, K. W.; Derfer, J. M.; Boord, C. E. *J. Am. Chem. Soc.* **1949**, *71*, 172.
(15) Brandrup, J.; Immergut, E. H., Eds.; *Polymer Handbook*; Wiley-Interscience: New York, 1975.
(16) Grassie, N.; Johnston, A.; Scotney, A. *Eur. Polym. J.* **1981**, *17*, 589.
(17) March, J. *Advanced Organic Chemistry*; Wiley-Interscience: New York, 1985; p 283.
(18) Higashimura, T.; Nishii, H. *J. Polym. Sci., Polym. Chem. Ed.* **1977**, *15*, 329.
(19) Kawakami, Y.; Toyoshima, N.; Yamashita, Y. *Chem. Lett.* **1980**, 13.

Theory of Crystallizable Block Copolymer Blends

Mark Douglas Whitmore*

Department of Physics, Memorial University of Newfoundland, St John's, Newfoundland A1B 3X7, Canada

Jaan Noolandi*

Xerox Research Centre of Canada, 2660 Speakman Drive, Mississauga, Ontario L5K 2L1, Canada. *Received August 26, 1987*

ABSTRACT: We present an equilibrium theory of blends incorporating diblock copolymers in which one of the copolymer blocks is crystallizable and the other is amorphous. The material is assumed to order in a lamellar structure of alternating semicrystalline and amorphous layers with the chemical bonds which connect the copolymer blocks lying in the interfacial regions between the layers. The amorphous blocks are modelled as flexible chains, each with one end (the joint) anchored in an interface. Their contribution to the free energy is calculated via the self-consistent solution of the modified diffusion equations. The crystalline regions are modelled as folded chains, also with one end in an interfacial region (bonded to the corresponding end of an amorphous block). In this paper, we specialize to the case of pure copolymer. We find that the calculated amorphous block free energies can be expressed as a single universal function depending on the total degree of polymerization of the amorphous block, its stretching, and a parameter proportional to the thickness of the interface. We have fitted an analytical form to this function, which can be used for any amorphous block, and we have combined it with our model of the crystallizable block to obtain an analytic expression for the lamellar thickness. As an example, the theory is applied specifically to PEO-*block*-PS copolymers.

1. Introduction

Block copolymers, one of whose components is crystallizable (for example, polyethylene oxide) while the other component is noncrystallizable (such as atactic polystyrene), have been studied extensively[1-11] and shown to possess equilibrium lamellar structures which can be obtained by annealing, usually in the presence of a preferential solvent for the amorphous domains. Unlike crystallizable homopolymers, where the chain folding is metastable, folding of the partly crystallizable blocks of copolymers exists at equilibrium, in which case it is governed by a balance of the thermodynamic forces between the crystalline and amorphous domains.[12] It is the purpose of this paper to give a detailed account of the origin of the various contributions to the overall free energy of such a system, thereby arriving at a theory of the equilibrium state. We carry out this program by further developing the statistical mechanics of inhomogeneous multicomponent polymeric systems, along the same lines as Hong and Noolandi,[13] and solving the appropriate mean field equations for the polymer chain distribution functions.

At first sight, the case of partly crystallizable block copolymers (we will assume diblock copolymers and lamellar morphology for the generic calculation given later) appears to be easier to treat than noncrystalline block copolymers, as we are clearly in the strong segregation limit, with no interpenetration of blocks and well-defined domain boundaries. However, the connectedness of the blocks of the copolymers imposes severe restrictions on the molecular conformations and gives rise to an intimate connection between the structural properties of the amorphous and crystalline domains. For example, at a given molecular weight and composition, compression of the amorphous domains can be accommodated to some extent by increasing the number of folds in the crystalline domains, thereby decreasing the average separation of the chain stems exiting from the crystalline region. The overall change in the free energy associated with this kind of molecular rearrangement is one of the main predictions of our theory. The equilibrium domain sizes are determined by packing constraints as well as the balance of the total energy of chain folding in the crystalline domains with the associated entropic conformational and stretching free energy of the noncrystallizable blocks in the amorphous domains.

The theoretical work presented in this paper is also of general interest for the understanding of the boundary conditions imposed on the solution of the modified diffu-

0024-9297/88/2221-1482$01.50/0

sion equation for the polymer distribution functions near a wall or abrupt interface. Other applications of this work are to the case of block copolymers or homopolymers adsorbed on surfaces and to the study of the wetting transition in a binary polymer mixture adjacent to and interacting with a surface. These topics will be covered in future publications.

In section 2 we give the general expressions for the free energy of segregated diblock copolymers, with one crystallizable and one amorphous block, in a multicomponent system including homopolymers and solvents. Most of the algebraic details of this section are included in Appendix A. Section 2 ends with a physical description of the various contributions to the free energy. Section 3 outlines the free energy calculation for the one-component system of diblock copolymers, and the self-consistent solutions of the modified diffusion equation for the amorphous block distribution functions are given in section 4. The numerical and analytical techniques required for the solution are summarized in Appendix B. Section 5 is devoted to a discussion of the crystalline free energy, and the calculated results for PEO-*block*-PS are presented in section 6. A comparison with available experimental data, and important scaling laws, are given in section 7, and section 8 contains the conclusions. The functional dependence of the free energy expression for the amorphous region is discussed in Appendix C.

2. Theory of Multicomponent Systems

In this section, we establish the general theory of the free energy of diblock copolymers consisting of one crystallizable and one amorphous block, blended with other components such as homopolymers and/or solvent molecules. In the first stages, we follow very closely the derivation of Hong and Noolandi,[13] with appropriate modifications for the crystallizable component. This is summarized in Appendix A.

We begin here with an expression for the free energy of the equilibrium morphology relative to a hypothetical uniform melt

$$\Delta F = \Delta W - \sum_{\kappa} \int \mathrm{d}^3 r\ \omega_\kappa(\mathbf{r})\rho_\kappa(\mathbf{r}) + \sum_{\kappa}^{\mathrm{C}} \tilde{N}_\kappa \ln \frac{\tilde{N}_\kappa Z_\kappa}{\bar{\mathbf{Q}}_\kappa \bar{\rho}_\kappa} - \sum_{\mathrm{C}} \tilde{N}_{\mathrm{C}} \ln \frac{e^{-\bar{\omega}_{\mathrm{CB}} z_{\mathrm{CB}}}}{\tilde{\bar{q}}_{\mathrm{CB}}(Z_{\mathrm{CB}})} \quad (2.1)$$

where $\omega_\kappa(\mathbf{r})$ and $\rho_\kappa(\mathbf{r})$ are the mean field and density, respectively, associated with component κ, Z_κ is the degree of polymerization, and $\tilde{N}_\kappa$ is the number of molecules. The bars over the letters all refer to the reference state, and $\mathbf{Q}_\kappa$ and q_κ are defined in terms of polymer distribution functions in Appendix A.

The interaction energy relative to the melt is given by

$$\Delta W = \tfrac{1}{2}\sum_{\kappa\kappa'} U_{\kappa\kappa'} \int \mathrm{d}^3 r\ [\rho_\kappa(\mathbf{r})\rho_{\kappa'}(\mathbf{r}) - \bar{\rho}_\kappa \bar{\rho}_{\kappa'}] - \frac{1}{12}\sum_{\kappa\kappa'} \sigma_{\kappa\kappa'}{}^2 U_{\kappa\kappa'} \int \mathrm{d}^3 r\ \nabla\rho_\kappa(\mathbf{r})\cdot\nabla\rho_{\kappa'}(\mathbf{r}) \quad (2.2)$$

The C over the summation sign in eq 2.1 indicates that for that sum, copolymers are to be treated as single components. The last sum in eq 2.1 represents the contribution from the crystallizable blocks. If all blocks were modelled as ideal flexible chains (i.e. amorphous copolymers), then we would have $\tilde{\bar{q}}_{\mathrm{CB}}(Z_{\mathrm{CB}}) = e^{-\bar{\omega}_{\mathrm{CB}} Z_{\mathrm{CB}}}$ as in eq A.40, and this sum would vanish.

These expressions are sufficiently general that they apply to systems containing one or more types of copolymers, hence the sum over copolymers in eq 2.1. We do, however, require all crystallizable blocks to be mutually compatible and all amorphous blocks to be so as well. Consequently, we expect this generality to be most useful for incorporating polydispersity, whereby molecules of different molecular weights but composed of the same chemical species can be treated as separate components.

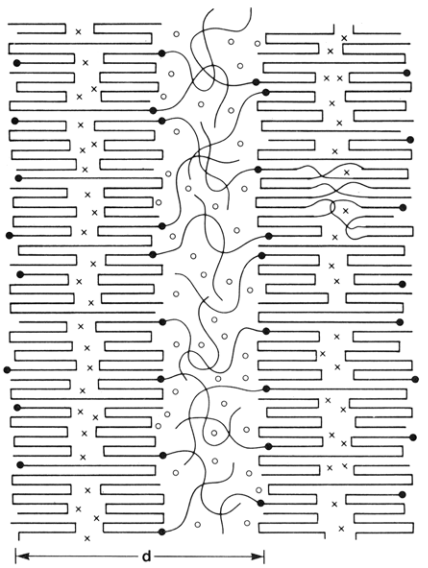

Figure 1. Lamellar structure of crystallizable block copolymer blend. The morphology consists of alternating layers.[1-5] One consists of the amorphous block of the copolymer plus compatible solvent (open circles). The other consists of the crystallizable block plus compatible solvent (small crosses). Although not shown, homopolymer can also be included. At equilibrium, the crystallizable blocks are folded and can in principle extend either one-half or all the way across the region. There can also be found amorphous portions of the crystallizable block (as indicated in the layer on the right). The chemical bonds joining the two blocks of each copolymer are localized to narrow interfacial regions.

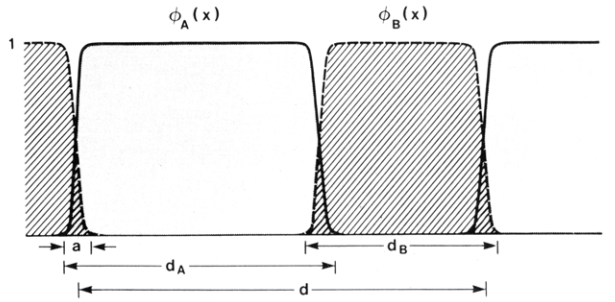

Figure 2. Volume fractions for the one-component copolymer system. The amorphous block is confined to alternating layers of width d_A and the crystallizable block to alternating layers of width d_B. The interfaces are of width a, and the total repeat distance is $d = d_A + d_B - 2a$. At all points, the local volume fractions sum to unity.

At this point, we introduce a specific model for the morphology.[1-4] As shown in Figure 1, we choose an infinite, periodic layered structure with a total repeat distance d. Each layer consists of two sublayers. One contains crystalline blocks including compatible solvent, and the other contains amorphous copolymer blocks, with homopolymers and/or compatible solvent. All copolymer joints are randomly distributed throughout the narrow interphase regions, each of which has a thickness a. Moving through the interphase, the amorphous component volume fractions fall smoothly to zero and the crystallizable component volume fraction rises to unity as shown in Figure 2 for a pure block copolymer system. At all points, the sum of all the volume fractions is unity.

Within each layer, the amorphous polymer extends over a distance d_A and the crystalline polymer over a distance

d_B. Each of these includes the interphase region, so the repeat distance is (see Figure 2)

$$d = d_A + d_B - 2a \tag{2.3}$$

If there are N layers, each with a cross-sectional area A, the total volume is $V = NAd$, and the density, distribution functions, and potentials are periodic, e.g.

$$q_\kappa(\mathbf{r},t) = q_\kappa(\mathbf{r} + d\hat{\mathbf{x}},t) \tag{2.4}$$

where the layers lie perpendicular to the x axis. The problem becomes one-dimensional, and we have from eq A.9

$$\mathbf{Q}_s = \frac{V}{d}\int_0^d dx\ e^{-\omega_s(x)} \tag{2.5}$$

for the solvent and from eq A.17

$$\mathbf{Q}_p = \frac{V}{d}\int_0^d dx\ q_p(x,Z_p) \tag{2.6}$$

for the homopolymer, with q_p satisfying the one-dimensional diffusion equation. It is convenient to rewrite these expressions as

$$\mathbf{Q}_s = V(d_A/d)\langle e^{-\omega_s}\rangle \tag{2.7}$$

$$\mathbf{Q}_p = V(d_A/d)\langle q_p(Z_p)\rangle \tag{2.8}$$

where the averages are over the amorphous region

$$\langle\psi\rangle = (1/d_A)\int_0^{d_A} dx\ \psi(x) \tag{2.9}$$

and the function being averaged [labeled generically $\psi(x)$] is nonzero only throughout the distance d_A. The overall particle densities are given by

$$\bar{\rho}_\kappa = N_\kappa Z_\kappa / V \tag{2.10}$$

Combining eq 2.7, A.29, and 2.10, we obtain for the solvent

$$\phi_s(x) = \bar{\phi}_s \frac{d}{d_A}\frac{e^{-\omega_s(x)}}{\langle e^{-\omega_s}\rangle} \tag{2.11}$$

where the macroscopic volume fraction of solvent is $\bar{\phi}_s = N_s/V$.

Similarly using eq 2.8 and eq A.30, we get for the homopolymer

$$\phi_p(x) = \bar{\phi}_p \frac{d}{d_A}\frac{1}{Z_p}\frac{\int_0^{Z_p} dt\ q_p(x,t)q_p(x,Z_p - t)}{\langle q_p(Z_p)\rangle} \tag{2.12}$$

The calculation of the periodic density distribution for the amorphous layers has therefore been reduced to a one-dimensional problem in *one* region of thickness d_A.

For the copolymers, we interpret $\tilde{q}_{CB}(\mathbf{r},Z_{CB})$ as proportional to the probability that the end of the crystallizable block which is bonded to the corresponding amorphous block is found in a small volume about the point $\mathbf{r}$. Since we assume the joints to be randomly and uniformly distributed throughout the narrow interphase regions, we have $\tilde{q}_{CB}(\mathbf{r},Z_{CB}) = 0$ if $\mathbf{r}$ corresponds to a point which is not in an interphase region and constant for $\mathbf{r}$ is inside any of the interphases. If we label the μ interfacial regions by Δ_μ, we can write

$$\tilde{q}_{CB}(\mathbf{r},Z_{CB}) = \tilde{q}_{CB}(Z_{CB})\sum_\mu \Delta_\mu(\mathbf{r}) \tag{2.13}$$

where

$$\begin{aligned}\Delta_\mu(\mathbf{r}) &= 1, \mathbf{r} \in \Delta_\mu \\ &= 0, \mathbf{r} \in \Delta_\mu\end{aligned} \tag{2.14}$$

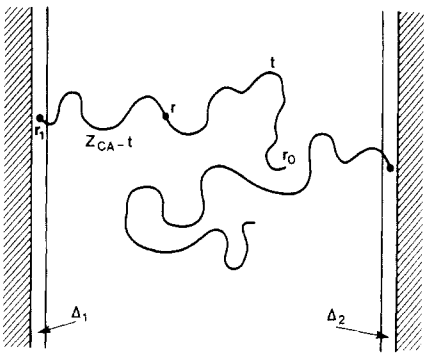

$$\rho_{CA}(r) \propto \sum_{\mu=1}^{2}\int_0^{Z_{CA}} dt \int_{\Delta_\mu} d^3r_1 \int d^3r_0\ Q_{CA}(r_1, Z_{CA}-t|r)\ Q_{CA}(r,t|r_0)$$

Figure 3. Convolution of probability functions for amorphous polymers.

The integral of the distribution function, eq A.18, then becomes

$$\mathbf{Q}_C = \tilde{q}_{CB}(Z_{CB})\sum_\mu \int_{\Delta_\mu} d^3r_1\ q_{CA}(\mathbf{r},Z_{CA}) \tag{2.15}$$

and the A block polymer density (eq A.31) is given by

$$\rho_{CA}(\mathbf{r}) = \frac{\tilde{N}_C}{\mathbf{Q}_C}\tilde{q}_{CB}(Z_{CB})\int_0^{Z_{CA}} dt\ q_{CA}(\mathbf{r},t) \times \sum_\mu \int_{\Delta_\mu} d^3r_1\ Q_{CA}(\mathbf{r},Z_{CA} - t|\mathbf{r}_1) \tag{2.16}$$

as shown schematically in Figure 3.

From the periodicity of q_{CA}, and its symmetry in each amorphous region, we have

$$\mathbf{Q}_C = 2N\tilde{q}_{CB}(Z_{CB})Aa\frac{1}{a}\int_0^a dx\ q_{CA}(x,Z_{CA})$$

$$\mathbf{Q}_C = 2V\tilde{q}_{CB}(Z_{CB})\left(\frac{a}{d}\right)\langle q_{CA}(Z_{CA})\rangle_a \tag{2.17}$$

where $\langle\ \rangle_a$ denotes an average over the interphase region of thickness a. For eq 2.16, we introduce new functions $q_{CA\mu}(\mathbf{r},t)$

$$q_{CA\mu}(\mathbf{r},t) = \int_{\Delta_\mu} d^3r_1\ Q_{CA}(\mathbf{r},t|\mathbf{r}_1) \tag{2.18}$$

These satisfy the usual modified diffusion equation, but with different initial conditions

$$q_{CA\mu}(\mathbf{r},0) = \Delta_\mu(\mathbf{r}) \tag{2.19}$$

The quantity $q_{CA\mu}(\mathbf{r},t)$ is proportional to the probability that a chain of length t ends at $\mathbf{r}$ given that it starts in Δ_μ.

In our model, no amorphous block penetrates *through* a crystalline region; therefore, in any amorphous layer, the density $\rho_{CA}(\mathbf{r})$ is due to chains anchored only in the two adjoining interphase regions. Thus for any point $\mathbf{r}$, only two terms contribute to the sum. We can now combine eq 2.16 and 2.17 to obtain

$$\phi_{CA}(x) = \phi_{CA1}(x) + \phi_{CA2}(x) \tag{2.20}$$

with

$$\phi_{CA\mu}(x) = \bar{\phi}_{CA}\frac{d}{d_A}\frac{1}{Z_{CA}}\frac{\int_0^{Z_{CA}} dt\ q_{CA}(x,t)q_{CA\mu}(x,Z_{CA} - t)}{2\langle q_{CA1}(Z_{CA})\rangle} \tag{2.21}$$

for $\mu = 1$ or 2. Here, we have used

$$\int_0^a q_{CA}(x,Z_{CA})\ dx = \int_0^{d_A} q_{CA1}(x,Z_{CA})\ dx \tag{2.22}$$

which follows from the definition of $q_{CA1}(x,Z_{CA})$ given by eq 2.18. Equation 2.20 shows the decomposition of the density in each amorphous region into two parts, each arising from blocks grafted to a side of the region, as shown schematically in Figure 3. The contribution from each side is expressed in a form analogous to that for the homopolymer except that for the homopolymer both ends are free, leading to the convolution $q_p{}^*q_p$, whereas for the copolymer block only one end ($t = 0$) is free and the other end ($t = Z_{CA}$) is in region μ, leading to the convolution $q_{CA}{}^*q_{CA\mu}$. The overall volume fractions $\bar{\phi}_\kappa$ in eq 2.11, 2.12, and 2.21 are determined by the molecular weights and concentrations in the sample.

The expressions for the $\mathbf{Q}_\kappa$ can now be inserted into the free energy function. Dividing by the total volume, as well as a reference density ρ_{0r}, we obtain for the reduced free energy per unit volume

$$\frac{\Delta F}{\rho_{0r}V} = \frac{\Delta W}{\rho_{0r}V} + \frac{1}{\rho_{0r}}\left\{\sum_s \rho_{0s}\left[\bar{\phi}_s \ln\left(\frac{d}{d_A}\right) + \frac{1}{d}\int_0^d dx\ \phi_s(x) \ln\frac{\phi_s(x)}{\bar{\phi}_s{}^a}\right] + \sum_p \rho_{0p}\left[\frac{\bar{\phi}_p}{Z_p}\ln\left(\frac{d}{d_A}\right) - \frac{\bar{\phi}_p}{Z_p}\ln\langle q_p(Z_p)\rangle - \frac{1}{d}\int_0^d dx\ \omega_p(x)\phi_p(x)\right] + \sum_C\left(\rho_{0C}\frac{\bar{\phi}_C}{Z_C}\ln\left(\frac{d}{2a}\right) + \rho_{0A}\left[-\frac{\bar{\phi}_{CA}}{Z_{CA}}\ln\langle q_{CA}(Z_{CA})\rangle_a - \frac{1}{d}\int_0^d dx\ \omega_{CA}(x)\phi_{CA}(x)\right] + \rho_{0B}\left[\frac{\bar{\phi}_{CB}}{Z_{CB}}\ln\frac{e^{\bar{\omega}_{CB}Z_{CB}}\tilde{\bar{q}}_{CB}(Z_{CB})}{\tilde{q}_{CB}(Z_{CB})} - \frac{1}{d}\int_0^d dx\ \omega_{CB}(x)\phi_{CB}(x)\right]\right)\right\} \quad (2.23)$$

Here $\bar{\phi}_s{}^a = (d/d_A)\bar{\phi}_s$ is the average solvent volume fraction in the amorphous layers. Each of the terms in this equation has a simple physical interpretation. The first term represents the change in the interaction energy of the lamellar structure relative to our hypothetical uniform melt. The next term refers to the entropy of the solvents. The first part of this term is due to configurational entropy loss arising from the overall restriction of the solvent molecules to a fraction (d_A/d) of the total sample volume. The second part is due to the nonuniform distribution of solvents within each layer. In the next bracket, the first part corresponds to the overall restriction of the homopolymers to the amorphous regions and the next two contributions arise from additional conformational and configurational entropy contributions. For the copolymers the localization of the joints to the interphases gives rise to a configurational entropy contribution. Since there are two interphases in each distance, d, the volume in which joints are found is a fraction $(2a/d)$ of the total. The last two lines are the configurational and conformational entropy terms for the amorphous and crystallizable blocks respectively.

3. Single-Component Copolymer Systems

In the remainder of this paper, we treat one component systems consisting of diblock copolymers with one amorphous (CA) and one crystallizable (CB) block, as shown in Figure 1, but with no solvent. Each ordered sublayer is assumed to consist of semicrystalline, chain-folded CB blocks. As shown in Figure 2, the volume fraction $\phi_{CB}(x)$ is equal to one throughout the interior of this region and falls smoothly to zero through the bordering interphases. Similarly, for the amorphous region $\phi_{CA}(x) = 1$ in the interior, falling to zero through the interphases such that $\phi_{CB}(x) + \phi_{CA}(x) = 1$ throughout. The overall volume fractions are related to the degrees of polymerization and pure component densities, e.g.

$$\bar{\phi}_{CA} = \frac{Z_{CA}\bar{\rho}_{0B}}{Z_{CA}\bar{\rho}_{0B} + Z_{CB}\rho_{0A}} \quad (3.1)$$

where $\bar{\rho}_{0B}$ is the average density of the pure, semicrystalline CB block

$$\frac{1}{\bar{\rho}_{0B}} = \frac{\tau}{\rho^c{}_{0B}} + \frac{(1-\tau)}{\rho^a{}_{0B}} \quad (3.2)$$

Here $\rho^c{}_{0B}$ is the density of crystallized CB material, $\rho^a{}_{0B}$ the density of the amorphous CB material, and τ the degree of crystallinity.

We assume that the thickness of the interphase is determined by the folds of the CB block. We do not attempt to calculate it here, rather we investigate its effect by carrying out free energy calculations for different values of the interphase thickness a.

For this system, the free energy, eq 2.23, reduces to

$$\frac{\Delta F}{\rho_{0A}V} = f_{cr} + f_{am} + f_{loc} + f_{int} \quad (3.3)$$

using ρ_{0A} as the reference density.

The first term is the crystallization energy of the CB block, which we identify as the last line of eq 2.23. Rather than attempt a first principles calculation of this term, we invoke a chain-folding model and choose

$$f_{cr} = \frac{\bar{\rho}_{0B}}{\rho_{0A}}\frac{\bar{\phi}_{CB}}{k_BT}\left[\frac{-\tau\Delta H_f}{\rho^c{}_{0B}} + \frac{n_f}{Z_{CB}}E_{fold}\right] \quad (3.4)$$

Here ΔH_f is the heat of fusion per unit volume of crystalline region, n_f is the number of folds per molecule, and E_{fold} is the energy per fold. The terms inside the brackets are the free energy per unit volume of crystalline region. This is multiplied by the overall volume fraction of CB material.

The next term in eq 3.3 is the contribution of the amorphous region. From eq 2.23 this can be written as

$$f_{am} = -\frac{\bar{\phi}_{CA}}{Z_{CA}}\ln\langle q_{CA}(Z_{CA})\rangle_a - \frac{1}{d}\int_0^d dx\ \omega_{CA}(x)\phi_{CA}(x) \quad (3.5)$$

f_{loc} is due to the localization of the joints:

$$f_{loc} = \frac{\rho_{0C}}{\rho_{0A}}\frac{1}{Z_C}\ln\left(\frac{d}{2a}\right) \quad (3.6)$$

and finally f_{int} is the change in interaction energy. Using the gradient expansion, we obtain

$$f_{int} = \chi_{AB}\left\{-\bar{\phi}_{CA}\bar{\phi}_{CB} + \frac{1}{d}\int_0^d dx\left[\phi_{CA}(x)\phi_{CB}(x) - \frac{\sigma^2}{6}\frac{d}{dx}\phi_{CA}(x)\frac{d}{dx}\phi_{CB}(x)\right]\right\} \quad (3.7)$$

where χ_{AB} is the Flory–Huggins interaction parameter defined by using ρ_{0A} as the reference density, $\chi_{AB} = \rho_{0B}U_{AB}$, and σ is the short-range parameter, $\sigma^2 = V_{AB}/U_{AB}$, which is assumed to be of molecular size, $\sigma = b_A$. The integrand in eq 3.7 is nonzero only in the interphase regions.

Evaluating f_{am} is by far the major task. For a given d, we solve for the polymer distribution function self-consistently to obtain $\langle q_{CA}(Z_{CA})\rangle_a$ etc. as shown in Appendix B. As discussed in the preceding section, for this part of the calculation we need consider one amorphous layer including the two bordering interphases. We define $\bar{\phi}^a_{CA}$ as the average of $\phi_{CA}(x)$ in this region (see eq 2.9) and $\bar{\phi}^a_{CA}$ is less than unity because it decreases rapidly in the interphase region. Since $\bar{\phi}^a_{CA} = (d/d_A)\bar{\phi}_{CA}$, we have

$$\phi_{CA}(x) = \phi_{CA1}(x) + \phi_{CA2}(x) \tag{3.8}$$

where

$$\phi_{CA\mu}(x) = \frac{\bar{\phi}^a_{CA}}{Z_{CA}} \frac{\int_0^{Z_{CA}} dt\ q_{CA}(x,t) q_{CA\mu}(x, Z_{CA} - t)}{2\langle q_{CA1}(Z_{CA})\rangle} \tag{3.9}$$

The distribution functions all satisfy the same differential equations and boundary conditions

$$\frac{\partial}{\partial t} q(x,t) = \left[\frac{b^2_A}{6} \frac{\partial^2}{\partial x^2} - \omega_{CA}(x) \right] q(x,t) \tag{3.10}$$

$$q(0,t) = q(d_A,t) = 0 \tag{3.11}$$

but different initial conditions

$$q_{CA}(x,0) = 1 \tag{3.12}$$

$$q_{CA1}(x,0) = \theta(a - x) \tag{3.13}$$

$$q_{CA2}(x,0) = \theta[x - (d_A - a)] \tag{3.14}$$

Since we assume that the volume fraction is unity between the interphases and is determined by the nature of the folding of the CB block via $\phi_{CA}(x) = 1 - \phi_{CB}(x)$ within the interphases, our procedure is to determine the unknown potential $\omega_{CA}(x)$ such that volume fractions as calculated by using eq 3.8–3.14 sum to unity at all points.

Our goal in this paper is to calculate the variations in $\Delta F/\rho_{0A}V$ with lamellar thickness d, but not its overall magnitude. That would require detailed knowledge of the reference (melt) state, the crystallization of the CB block, and the fold surfaces. Without this information, we do not know the density profile of $\phi_{CA}(x)$ in the interphases. However, we need only to ensure that we do not introduce spurious variations in $\phi_{CA}(x)$ as we vary d_A. Hence, we first complete the full self-consistent calculation for one value of d_A, requiring only that $\phi_{CA}(x) = 1$ in the interior region, $a \le x \le d_A - a$, with $\phi_{CA}(0) = \phi_{CA}(d_A) = 0$. This calculation yields profiles $\phi_{CA}(x)$ in the two subintervals $[0,a]$ and $[d_A - a, d_A]$. In all subsequent calculations, these profiles, together with $\phi_{CA}(x) = 1$ in the interior region, were used as the "target" $\phi_{CA}(x)$.

It is useful to note that in solving the self-consistent equations, there is no reference to the crystalline regions. Indeed we can rewrite eq 3.5 as

$$f_{am} = \bar{\phi}_{CA} \left[-\frac{1}{Z_{CA}} \ln \langle q_{CA}(Z_{CA})\rangle_a - \frac{1}{d_A \bar{\phi}^a_{CA}} \int_0^{d_A} dx\ \omega_{CA}(x)\phi_{CA}(x) \right] \tag{3.15}$$

The part in the brackets depends only on the amorphous region; the crystalline part enters through the prefactor. In fact, it is not difficult to show (see Appendix C) that this entire term can be written in the functional form

$$f_{am} = (\bar{\phi}_{CA}/Z_{CA}) g_\gamma(\alpha) \tag{3.16}$$

where

$$\alpha = (3/Z_{CA})^{1/2}(d_A/b_A) \tag{3.17}$$

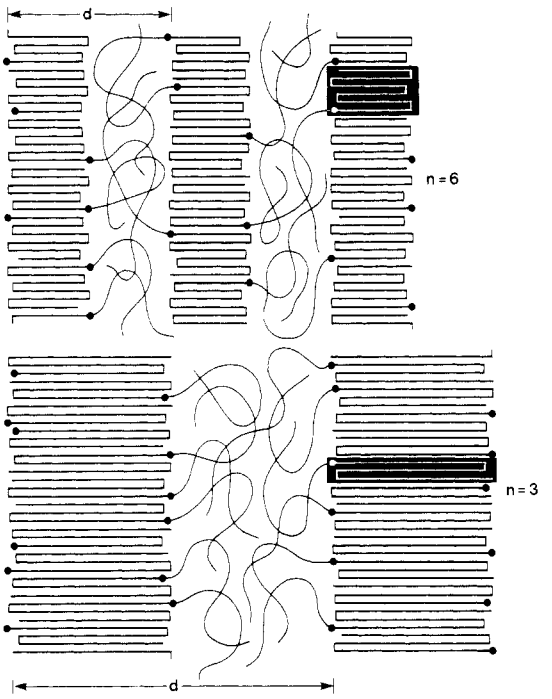

Figure 4. Effects of changes in layer thickness. For relatively thin layers (upper diagram), there are many folds per crystallizable block and the joints at each interface are on average relatively far apart. n denotes the number of folded sections of the crystallizable block. The amorphous blocks each extend fully across the (narrow) amorphous region. For thicker layers (lower diagram), the crystallizable block partially unfolds and the joints are closer together. The amorphous blocks each reach to only about the midpoint of the domain (see Figures 5 and 6 for further discussion).

is a measure of the thickness of the region relative to unstretched blocks and

$$\gamma = (1/Z_{CA})^{1/2}(a/b_A) \tag{3.18}$$

is a measure of the thickness of the interphase relative to the unperturbed chain.

Using eq 3.3 and 3.16, we can identify $g_\gamma(\alpha)$ as the free energy per molecule of the amorphous region. Once it is known, it can be used for amorphous blocks of any Kuhn length b_A, degree of polymerization Z_{CA} and reference density ρ_{0A}. As well, it can be used in conjunction with any crystallizable block to provide a description of any partly crystalline copolymer. The connection between the two blocks is through the joints whose density per unit area in the interphase region is

$$\delta = (d/2Z_C)\bar{\rho}_{0C} \tag{3.19}$$

Increasing d implies an increase in δ as illustrated in Figure 4. Partitioning each interphase into equal halves associated with the adjoining layers, the overall thicknesses of the amorphous and crystalline layers are given by

$$\tilde{d}_A = \bar{\phi}_{CA} d \tag{3.20}$$

$$\tilde{d}_B = \bar{\phi}_{CB} d \tag{3.21}$$

where $\tilde{d}_A = d_A - a$ and $\tilde{d}_B = d_B - a$ consistent with eq 2.3.

4. Self-Consistent Calculations for the Amorphous Region

We have carried out self-consistent calculations for values of the interphase thickness parameter, γ (eq 3.18), equal to 0.05, 0.10, 0.15, and 0.20, with the lamellar thickness parameter, α (eq 3.17), varying from about 1 to nearly 8. For all calculations in this paper, we have taken the range of the potential to be zero ($\sigma = 0$). The detailed procedure is discussed in Appendix B. Typical density

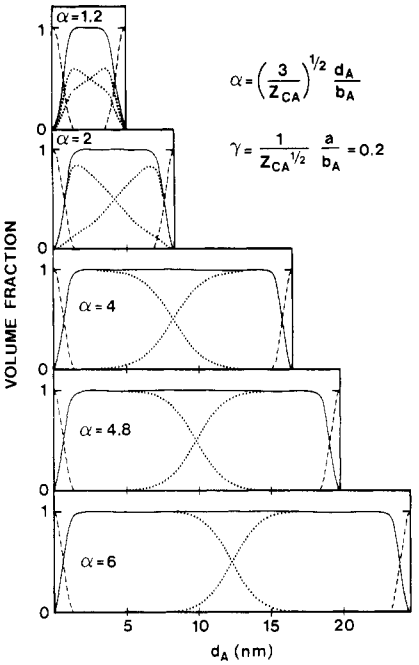

Figure 5. Variations in polymer volume fraction with domain thickness d_A for $\gamma = 0.20$, corresponding to the schematic diagram shown in Figure 4. The distance scale at the bottom corresponds to PS blocks with $Z_{CA} = 100$, for which case the interphase has thickness $a = 2b_A$. The top panel shows the case of a narrow layer ($\alpha = 1.2$) and low surface density of graft points at each side, with the amorphous blocks squeezed by the crystallizable blocks. The lower panels correspond to higher surface densities of graft points, and larger α. For $\alpha > 4$, each block reaches only to about the middle of the domain and must stretch in so doing.

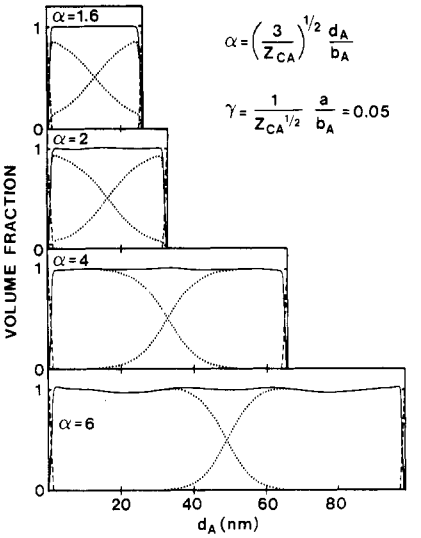

Figure 6. Variations in polymer volume fraction with domain thickness for $\gamma = 0.05$. Particularly for $\alpha > 4.0$, the individual profiles are nearly the same as for $\gamma = 0.20$ in Figure 5, except near the crystalline wall. The distance scale corresponds to PS blocks with $Z_{CA} = 1600$, in which case $a = 2b_A$.

profiles are shown in Figures 5 and 6.

Figure 5 shows density profiles for the case $\gamma = 0.20$ and five values of α ranging from 1.2 to 6. The distance scale that is included is for the particular case $Z_{CA} = 100$, in which case the interphase has thickness $a = 2b_A$. The profiles themselves apply to any value of Z_{CA}. For example, for $Z_{CA} = 400$ we would have $a = 4b_A$, and the distance scale would be doubled (out to about 49 nm for $\alpha = 6$).

The uppermost panel is for $\alpha = 1.2$. This corresponds to relatively small d_A and low surface density of graft points at each side. We see that the total volume fraction of amorphous copolymer increases from zero at $x = 0$ to unity at $x = a$, remains at unity until $x = d_A - a$, and then decreases to zero at $x = d_A$. Each individual contribution, ϕ_{CA1} and ϕ_{CA2}, peaks near the corresponding boundary region but is zero only at the ends. This implies that each block reaches across the entire region, although not with uniform volume fraction.

Increasing α (subsequent panels in Figure 5) corresponds to larger d_A and increased surface density of graft points. Consequently, the peaks in the individual ϕ_{CA1} and ϕ_{CA2} are higher, and the corresponding profiles do not reach completely across the interval. For $\alpha \geq 4$, the peaks have reached unity, and the individual blocks reach only part way across. As α increases further, the peaks become plateaus, so that ϕ_{CA1} and ϕ_{CA2} are each unity over a finite range. Of course the total volume fraction ϕ_{CA} is unity throughout the range $x \in [a, d_A - a]$ within the accuracy of the calculation. It is interesting to note also that once the interval is sufficiently large that each block does not reach to the far interphase, the profiles of ϕ_{CA1} and ϕ_{CA2} at the center of the domain are independent of α. Only the extent of the plateaus changes in this regime.

Figure 6 shows similar results, but for the much more narrow interphase corresponding to $\gamma = 0.05$. Again, we include a distance scale, but this time corresponding to $Z_{CA} = 1600$, implying an interphase of thickness $a = 2b_A$. As for Figure 5, this can be used for other values of Z_{CA} implying rescaled distances. Otherwise, the behaviour is similar to that shown in Figure 5, except for the more rapid rise (relative to the entire interval) in the volume fractions. A small difference is that, in this case, plateaus have developed for $\alpha = 4$, whereas they were just beginning to appear for this value of α in Figure 5. Note that for $\alpha \geq 4$, the individual profiles at the center are nearly identical for the two cases ($\gamma = 0.05$ and $\gamma = 0.20$), when plotted as a function of α. The width of the overlap region is seen to be

$$d_I \simeq (Z_{CA}/3)^{1/2} b_A \tag{4.1}$$

independent of both α and γ (and hence the interphase thickness) but clearly dependent on Z_{CA}.

We have included the bottom panel to illustrate the limitations on the calculations at large α. As the molecules are forced into conformations such that the volume fractions ϕ_{CA1} and ϕ_{CA2} equal unity over larger regions, it becomes more and more difficult to achieve self-consistent solutions. The difficulty appears as oscillations in ϕ_{CA} near the center of the interval. As discussed in Appendix B, we included the results only if the mean squared error in the converged solutions was less than 0.02.

We can quantify the stretching of the individual molecular blocks by calculating the reduced weighted average

$$x_{red} = \left(\frac{3}{Z_{CA}}\right)^{1/2} \frac{\langle x^2 \rangle^{1/2}}{b_A} \tag{4.2}$$

where

$$\langle x^2 \rangle^{1/2} = \frac{\int_0^{d_A} dx\, x^2 \phi_{CA1}(x)}{\int_0^{d_A} dx\, \phi_{CA1}(x)} \tag{4.3}$$

Figure 7 shows x_{red} as a function of α. It varies from $x_{red} \simeq 0.5\alpha$ for small α to $x_{red} \simeq 0.3\alpha$ for large α. There are three scaling regimes, summarized by

$$\begin{aligned} x_{red} &\approx \alpha, \quad \alpha \lesssim 1 \\ &\approx \alpha^{0.5}, \quad 2 \lesssim \alpha \lesssim 3 \\ &\approx \alpha, \quad \alpha \gtrsim 4 \end{aligned} \tag{4.4}$$

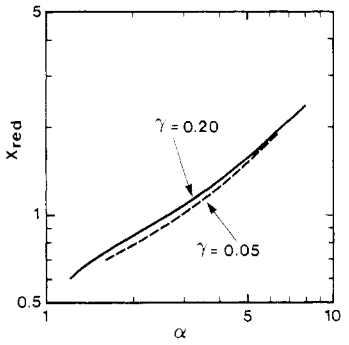

Figure 7. Extension of amorphous blocks as a function of the scaled domain thickness $\alpha = (3/Z_{CA})^{1/2} d_A/b_A$. The extent of the blocks grafted to each side is measured by x_{red}, as defined in eq 4.2. For very small α ($\alpha < 1$), each block extends fully across the narrow domain, and x_{red} scales approximately linearly with α. As α is increased, the blocks expand more slowly, until $\alpha \simeq 4$. Beyond this value, each profile reaches to the middle, and x_{red} again scales approximately linearly with α.

We can understand these results from Figure 5. For $\alpha \gtrsim 4$ each molecule extends approximately to the midpoint, and as noted before the profiles in the overlap region are nearly independent of α; thus x_{red} must scale linearly with α. For $1 \lesssim \alpha \lesssim 4$, the individual profiles change as α changes, and x_{red} varies more slowly, scaling approximately with $\alpha^{0.5}$ over part of the interval. For $\alpha \lesssim 1$, each block is constrained by both boundaries of the domain, and as α is reduced, the blocks are compressed; once again, x_{red} scales linearly with α.

It is easy to show that in the limiting case of very large α in which each molecular distribution fills one half the region, then

$$x_{red} \simeq 0.3\alpha \tag{4.5}$$

In the other limit of small α in which each molecule extends uniformly over the entire domain, ϕ_{CA1}, $\phi_{CA2} = {}^1/_2$ throughout, and

$$x_{red} \simeq 0.6\alpha \tag{4.6}$$

These limits are not reached in our calculations. But on this basis, we would expect the ratio x_{red}/α to fall from near 0.6 for small α to 0.3 for large α. Once this ratio reaches 0.3, x_{red} should scale linearly with α. This is in agreement with the full calculations. We now turn our attention to the free energy function $g_\gamma(\alpha)$, shown in Figure 8. The four curves correspond to the four values of the parameter γ; the actual value of the interphase thickness can be calculated from eq 3.18. For example, with $Z_{CA} = 100$, the four curves correspond to $a = 0.5b_A$, b_A, $1.5b_A$, and $2b_A$. For $Z_{CA} = 400$, they correspond to $a = b_A$ and larger values of a.

Consider first the α dependence. Each curve has a minimum, occurring near $\alpha \simeq 4$ (depending on γ). If there were no driving force due to the folding of the crystalline block, then this alone would determine the equilibrium d_A and hence the overall d. Using x_{red} as a measure of the stretching of the individual molecules, we find that this minimum occurs at

$$x_{red} \simeq 1 \tag{4.7}$$

which describes the x component of the root-mean-square end-to-end distance of an *unperturbed* chain.

There is also an increase in g with decreasing γ; i.e., as the interphase is made narrower, the free energy f_{am} increases. This is reasonable because the volume fraction $\phi_{CA}(x)$ must rise more steeply and remain constant (equal to one) over a greater distance (see Figures 5 and 6). The

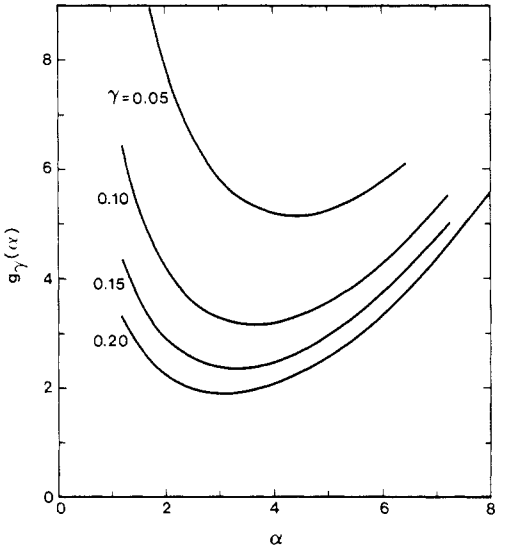

Figure 8. Plot showing $g_\gamma(\alpha)$, a universal function of γ and α which corresponds to the interphase thickness and amorphous domain width, respectively, relative to the dimensions of the unperturbed block. With this function, f_{am} can be calculated for any Z_{CA}, b_A, or ρ_{0A} and hence for any amorphous block.

Table I
Summary of Free Energy Calculations for the Amorphous Region

$$g_\gamma(\alpha) = \frac{A}{\sqrt{\gamma}}\alpha^\mu + \frac{B}{\gamma\alpha} + C$$

surface parameter γ	A	μ	B	C
0.05	0.0159	2.11	0.740	0.13
0.10	0.0160	2.24	0.739	0.21
0.15	0.0158	2.33	0.731	0.23
0.20	0.0171	2.34	0.730	0.19

number of possible molecular conformations clearly decreases as these constraints become more severe, leading to higher free energies. Physically, one might anticipate that g could be described by a Flory-type expression including the elastic free energy and the interfacial tension

$$g \simeq C_1\alpha^\mu + C_2/\alpha + C_3 \tag{4.8}$$

This expression fits the curves shown in Figure 8 with root-mean-square errors of about 10^{-3} over the entire range of α. In fact C_1, C_2, and C_3 scale with γ in a simple way, at least for $\gamma \leq 0.15$. Writing eq 4.8 as

$$g \simeq \frac{A}{\sqrt{\gamma}}\alpha^\mu + \frac{B}{\gamma\alpha} + C \tag{4.9}$$

then A, B, and C are nearly independent of γ and are listed in Table I. For completeness, we have included in Table I the constant C even though it is insignificant in the larger α regions which are of interest in the copolymer problem. With eq 4.9, we can extrapolate $g_\gamma(\alpha)$ to larger α and interpolate and extrapolate to values of γ.

Equation 4.9 can be compared with previous work on amorphous copolymers. Using the definitions of α and γ, absorbing factors of $\sqrt{3}$ into new constants A' and B', and dropping the last term, we can rewrite g as

$$g \simeq A'\left(\frac{b_A\sqrt{Z_{CA}}}{a}\right)^{1/2}\left(\frac{d_A}{b_A\sqrt{Z_{CA}}}\right)^\mu + B'\left(\frac{b^2_A}{a}\right)\frac{Z_{Ca}}{d_A} \tag{4.10}$$

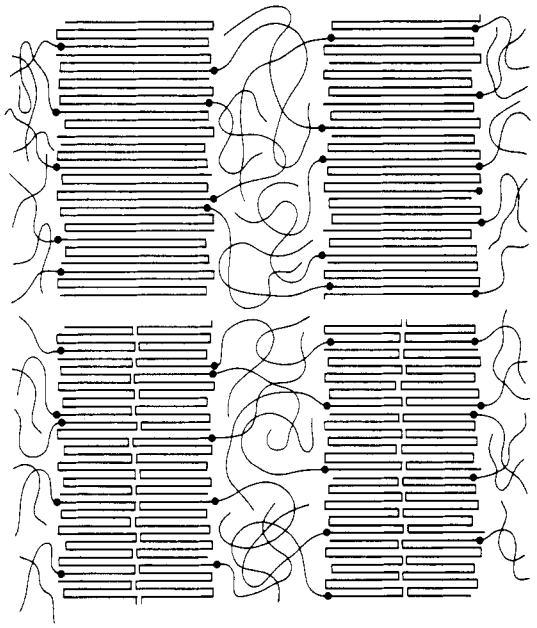

Figure 9. Model morphologies. In the single-layer model (upper half of figure) each PEO block extends fully throughout the domains, and folds occur only in the interphase regions between domains (ref 1 and 2). In the double-layer model (ref 3–11), each PEO block reaches, on average, halfway across the domain, and the number of folds per molecule is approximately doubled. There may be noncrystalline regions within the PEO blocks. Note that for a given thickness d_B, the surface area per joint (δ in eq 3.19), and the thickness of the amorphous layer, d_A, are the same for the two models. The free energy is higher for the double-layer model than for the single-layer model because of the additional folds.

Helfand and Wasserman,[14] Semenov,[15] and Ohta and Kawasaki[16] found corresponding results

$$g \simeq A'\left(\frac{d_A}{b_A\sqrt{Z_{CA}}}\right)^{\mu} + B'b_A\frac{Z_{CA}}{d_A} \qquad (4.11)$$

Helfand and Wasserman[14] numerically found $\mu = 2.5$, whereas in the limit of infinite molecular weight Semenov[15] and Ohta and Kawasaki[16] analytically found $\mu = 2$. In this work, we find $\mu = 2.3$ for small Z_{CA} ($\gamma = 0.20$), decreasing toward $\mu = 2$ for larger Z_{CA} (decreasing γ). We also find explicit dependence on the interphase thickness in both terms; Ohta and Kawasaki[16] found the same dependence for the second term.

5. Crystalline Free Energy

We model the crystalline region as a semicrystalline layer of folded CB blocks. In order to calculate the free energy f_{cr}, we need to know the crystallinity τ, the number of folds per molecule n_f, the heat of fusion ΔH_f, and fold energy E_{fold}.

We investigate two models for the crystalline layer,[4,9,17] which are shown in Figure 9. The first, which we call the "single-layer model" is shown in the upper half. Each CB block traverses the entire crystalline layer, with no folds in the interior. There may be some noncrystalline parts; we characterize this by the degree of crystallinity, τ. The geometry of this model allows for layer thicknesses such that the free end of a CB block terminates either in the CB–CA interphase or in the center of the crystalline region. If n denotes the number of segments per molecule (traverses of the crystalline layer) and L_B is the extension of a fully extended block perpendicular to the lamellar face, then $n = L_B/d_B$ can be integer or half-integer. The number of folds per molecule is then

$$\begin{aligned} n_f &= L_B/d_B - 1 \quad n \text{ integer} \\ &= L_B/d_B - \tfrac{1}{2} \quad n \text{ half-integer} \end{aligned} \qquad (5.1)$$

In practice, there may be "end effects" which we have neglected, but which force the free ends to lie at the lamellar surfaces. However, anticipating the results of sections 6 and 7, we find that in all cases our model gives the lowest free energy for the case of integral n, so that even without end effects the equilibrium morphology corresponds to the free end being at the surface.

The second model, which we call the "double-layer model", is shown in the bottom half of Figure 9. Each CB block traverses only part way through the layer, before folding back. This morphology is suggested by the work of Gervais and Gallo,[9,10] who obtained electron micrographs of freeze fractures occurring preferentially in the centers of the crystalline block.

For fully crystalline CB blocks, the single-layer model has the lowest free energy because for a given d_B there is less folding. This would imply that the double-layer structure occurs because of nonequilibrium effects. However, this might not be the case for semicrystalline CB blocks. Because the noncrystalline CB material is found to be concentrated in the middle of the CB layer, the fold energy associated with the inner surface may be reduced. In the extreme, there may be none at all, in which case the only fold surface is at the CB–CA interphase and the fold energy is the same as for the single-layer model. In practice, we expect at least some fold energy to be associated with the interior region.

In order to address this question theoretically, we need a detailed analysis of the semicrystalline regions, which we do not undertake. Instead, we shall consider two cases, namely, the single layer model and the double-layer model with complete folding in both regions. We note that the results for the extreme example of the double-layer model but with no folding in the inner regions are nearly identical with those for the single-layer model (because the number of folds per molecule is the same).

We assume that the crystallinity τ is independent of lamellar thickness. This may not be the case in nonequilibrium samples in which the kinetics of growth may determine both lamellar thickness and τ. However, we are unaware of any evidence to suggest that at equilibrium τ varies with d. With this assumption, the product $\tau\Delta H_f$ is independent of d, and the d dependence of f_{cr} is due solely to the folds. We denote this contribution by f_{fold}.

6. PEO-*block*-PS

In this section, we apply the formalism to the specific case of PEO-*block*-PS.[1–5,9–11] Unfortunately, there is a paucity of experimental *equilibrium* data; with one possible exception, all of the quoted results are for samples not in thermodynamic equilibrium.

For the amorphous free energy, we use the calculated $g_\gamma(\alpha)$ of section 4. We take for the density of pure PS[18]

$$\rho_{0A} = 5.782/\{0.9199 + 5.098 \times 10^{-4}(T - 273) + 2.354 \times 10^{-7}(T - 273)^2 + [32.46 + 0.1017(T - 273)]/M\} \text{ nm}^{-3} \qquad (6.1)$$

where T is the temperature in kelvins and $M = 104.15Z_{CA}$ is the molecular weight of the PS block.

For the PEO block, we use $\rho^{\alpha}_{0B} = \rho^{c}_{0B}$; i.e. the amorphous and noncrystalline PEO densities are equal. The crystal structure[19] is monoclinic, with the unit cell c axis of length $c = 1.93$ nm. The volume of the unit cell is 1.653 nm^3. Four chains spiral through, each in a helical structure containing seven monomers and two turns (7_2 helix). Thus, $\rho^{c}_{0B} = 16.9$ nm^{-3}.

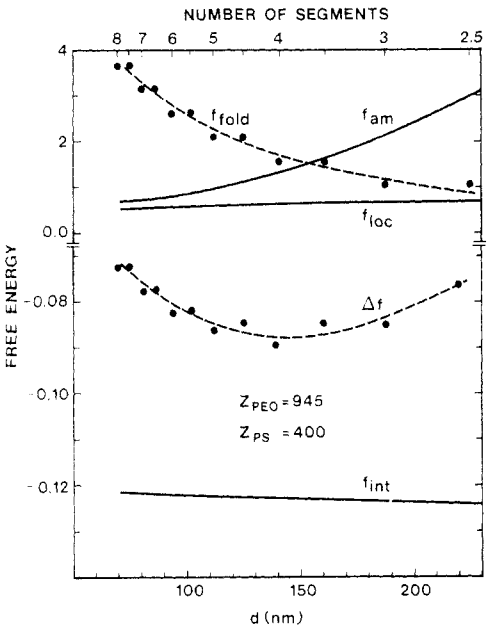

Figure 10. Theoretically calculated individual contributions to the free energy for PEO-*block*-PS with $Z_{PEO} = 945$ and $Z_{PS} = 400$ and interphase thickness $a = b_A$, for the single-fold model. The copolymer here has equal molecular weight blocks. We plot the free energy due to the folds, f_{fold}, for only integer and half-integer values of the number of segments of the crystallizable block but the other contributions as continuous functions of the total lamellar thickness d. The total free energy, Δf, is the sum of the four contributions shown; for convenience, we have not included the constant term due to the heat of fusion. For this case Δf is a minimum at $n = 4$, corresponding to a thickness $d = 141$ nm.

To calculate the energy, we need to know the number of folds per molecule. In the single-layer model, the number of segments per molecule is

$$n^s = \frac{Z_{CB}}{7}\,\frac{c}{d_B}\,\frac{\rho^c{}_{0B}}{\bar{\rho}_{0B}} \tag{6.2}$$

and the number of folds per molecule is given by eq 5.1. Note that since the crystallographic distance c accommodates seven monomers per chain, fully extended, perfectly crystalline chains would produce $d_B = (Z_{CB}/7)c$, and there would be no folds.

In the double-layer model, the number of segments per molecule is twice as large

$$n^d = \frac{Z_{CB}}{7}\,\frac{c}{d_B/2}\,\frac{\rho^c{}_{0B}}{\bar{\rho}_{0B}} \tag{6.3}$$

Finally we choose $\Delta H_f = 2.33 \times 10^{-19}$ J nm^{-3}, and $E_{fold} = 1.6 \times 10^{-20}$ J.[17] As discussed above, the value of ΔH_f does not affect our prediction of the equilibrium spacing. However, since it is the folding energy which drives the system toward larger d, our results do depend on the value of E_{fold}.

The last quantity we need is the interaction parameter χ_{AB}. Here we take $\chi_{AB} = 0.5$, which is the value for PS–PDMS since the value for PS–PEO is not readily available. As we shall discuss below, any error here is insignificant since f_{int} is almost completely independent of d.

In Figure 10, we show typical results for all the contributions to the free energy for the single-layer model for the case of $Z_{PEO} = 945$ and $Z_{PS} = 400$ and an interphase thickness $a = b_A$ (d_{cr} is replaced by f_{fold} since we have not included the large but constant heat of fusion term). The values of Z_{PEO} and Z_{PS} correspond to a 50/50 copolymer by weight. Note the slow, logarithmic increase in f_{loc} and the very slow decrease in f_{int} with increasing d, arising from the constant interphase thickness as d changes. The amorphous free energy contribution grows with increasing d because of the greater stretching, whereas f_{fold} decreases, due to the unfolding of the molecules for larger d. The total free energy has a minimum corresponding to four segments or three folds per chain. It is clear that only f_{fold} and f_{am} determine the equilibrium spacing.

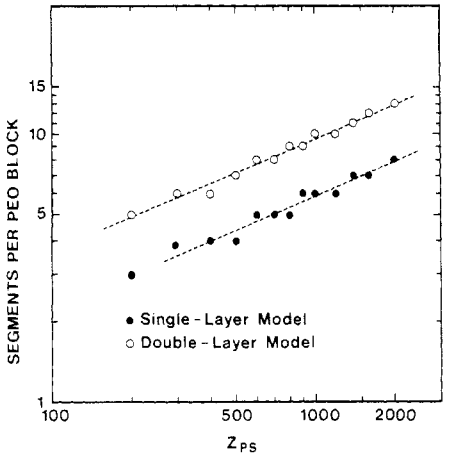

Figure 11. Theoretically calculated equilibrium number of segments per PEO block as a function of Z_{PS}, for $a = b_A$. The results are independent of the degree of polymerization of the PEO block; this figure applies for any Z_{PEO}. For given Z_{PS}, we find approximately 1.6 times the number of segments in the double-layer model as in the single-layer model. In either model, n_{eq} scales approximately as a power of Z_{PS}; the dotted lines correspond to a power of 5/12 (see section 7).

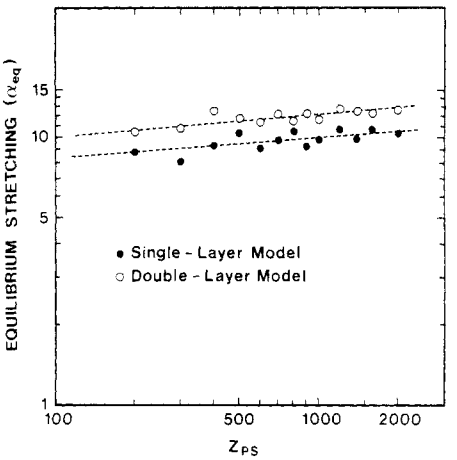

Figure 12. Theoretically calculated equilibrium thickness of the amorphous layer relative to the unperturbed PS block, for $a = b_A$. As for the number of equilibrium segments of the PEO block, α_{eq} is independent of Z_{PEO}. The apparent irregularity of α_{eq} is due to the integer values of n_{eq}. However, there is a general increase in α_{eq} with Z_{PS}. The dotted lines through the calculated points correspond to a power law relationship with a power of about 1/12 (see section 7). For given Z_{PS}, α_{eq} for the double-layer model is increased by a factor of 1.25 relative to its value for the single-layer model.

Figures 11–13 exhibit the main numerical results of this section. They illustrate the equilibrium values of the number of segments per crystallizable block, n_{eq}, the thickness of the amorphous layer relative to the unperturbed amorphous block, α_{eq}, and the total repeat distance, d_{eq}. We show results for the single- and double-layer models. The calculations were done for degrees of polymerization $Z_{PEO} = 400$ and $Z_{PEO} = 1600$ and for each of these cases for Z_{PS} in the range $200 \le Z_{PS} \le 2000$. We do not expect that copolymers with highly disparate blocks, e.g., $Z_{PEO} = 400$ and $Z_{PS} = 2000$, necessarily form lamellae.

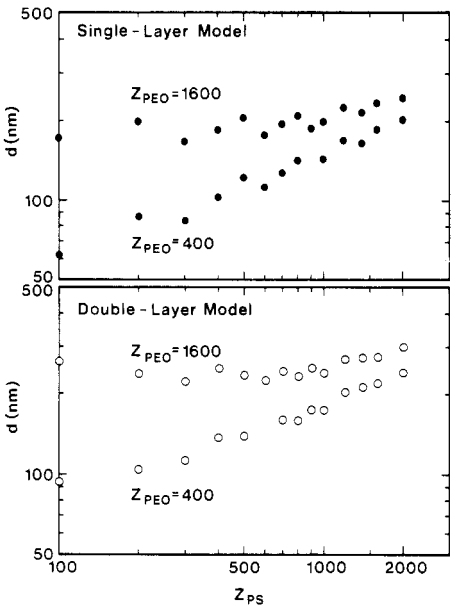

Figure 13. Theoretically calculated equilibrium repeat distance as a function of molecular weight for single-layer model (upper panel) and double-layer model (lower panel). In all cases, if $Z_{PS} > Z_{PEO}$, d increases with increasing Z_{PS}. However, for $Z_{PS} > Z_{PEO}$, d is approximately 1.25 times larger for the double-layer model than for the single-layer model.

However, we do not attempt to calculate where possible morphological changes might occur.

Consider first Figure 11, which shows the number of segments per PEO block as a function of Z_{PS} for both the single- and double-layer models. Note first that the results for $Z_{PEO} = 400$ and for $Z_{PEO} = 1600$ are identical. In fact, this is an example of a general result; in all our results n_{eq} is independent of Z_{PEO}. In addition, n_{eq} is always integral. This might be the case for the double-layer model, or else the joints would not all be in the interphases. As discussed above, for the single-layer model n_{eq} could in principle be half-integral; this can be analyzed as follows. To begin, consider an integral number of folds, n. If the layer thickness were increased slightly so that n is replaced by $n - {}^1/_2$, then there would be no change in the number of folds per PEO block. However, each PS block would have to be more stretched, leading to a higher free energy. On the other hand, if the layer thickness were decreased slightly so n is replaced by $n + {}^1/_2$, then one additional fold per CB block would be introduced, and the fold energy increased. The PS block would be less stretched, but in all cases we find that the increase in fold energy is greater than the reduction in f_{am}, and an integral number of segments always minimizes the free energy (even neglecting end effects). Next note that for a given Z_{PS}, the double-layer model has approximately 1.6 times the number of segments as the single-layer model. This implies that the layer thickness is approximately 1.25 times smaller for the single-layer model.

Since n_{eq} is not continuous, the values do not fall precisely on any smooth curve. However, in Figure 11 they lie near a straight line, approximating a power law relationship $n_{eq} \propto Z_{PS}^{\nu}$, with $\nu \simeq 0.4$ for each model as illustrated. This is discussed further in the next section.

Figure 12 shows α_{eq} vs Z_{PS} for the amorphous region. Since $6 < \alpha_{eq} < 12$, we are at least in some cases extrapolating the calculated $g_\gamma(\alpha)$. Note that α_{eq} is not a continuous function (due to the integral changes in n_{eq}). However, the results are consistent with an approximate but weak dependence $\alpha_{eq} \propto Z_{PS}^{\omega}$, where $\omega \simeq 1/12$. For the double-layer model, α_{eq} is about 1.25 times larger than for the single-layer model. Again, we emphasize that α_{eq} is independent of Z_{PEO}.

Figure 13 shows the repeat distance d as a function of Z_{PS} for the single-layer (upper panel) and double-layer (lower panel) models. Since it is the number of segments, n_{eq}, which is independent of Z_{PEO}, the thickness of crystalline layer, d_B, scales linearly with Z_{PEO}, and so d depends on both Z_{PEO} and Z_{PS}. Note that for $Z_{PEO} \leq Z_{PS}$, this dependence is slower or possibly even reversed. This is suggested, in particular, for the case of $Z_{PEO} = 1600$ in each model. Comparing the two models, d is always larger for the double-layer model than for the single-layer model.

7. Discussion

In a series of papers, Gervais, Gallot, et al.[4-11] examined the morphology of crystallizable block copolymers with and without solvent preferentially soluble in one of the blocks. They studied PEO-*block*-PS, PEO-*block*-PBD, and PCL-*block*-PS, in which PEO and PCL formed the semicrystalline blocks. In particular, they looked at the effects of different molecular weights, solvent concentrations, crystallization temperatures, and crystallinity and measured chain folding and lamellar thickness. Most of their data appear to be for nonequilibrium samples. Also, because of polydispersity, the ends of at least some PEO blocks must be within the crystalline layers and some folding occurs within the layers. Finally, they interpret their results using the double-layer model. In spite of these difficulties, it is interesting to compare our results with overall trends which they have identified.

First, the crystallized structure is always found to be lamellar, as we have assumed. Second, they find that the variation in crystallinity τ with the amount of folding is less than can be observed experimentally, consistent with our assumption that τ is independent of d as discussed in section 5. The PEO and PCL folding was found to depend on the relative molecular weights of the two blocks and the crystallization temperature. In particular, for PEO-*b*-PS, with fixed Z_{PEO} the number of folds per block, n_f, increases with Z_{PS}; for less than 50% PEO by weight, n_f is independent of Z_{PEO} and is determined solely by Z_{PS}. For larger PEO content, n_f increases with both Z_{PS} and Z_{PEO}. The number of folds decreases with increasing crystallization temperature, an indication of nonequilibrium effects. With $Z_{PEO} = 125$ and $Z_{PS} = 34$, Gervais and Gallot[4] find $n_f = 8$ at a crystallization temperature $T_C = 10$ °C, decreasing to $n_f = 5$ at $T_C = 43$ °C. Using the double-layer model, for these degrees of polymerization, we calculate $n_f = 2$ if we assume complete folding at both surfaces and $n_f = 3$ if we assume there is no fold energy associated with the amorphous PEO in the interior of the semicrystalline layer. The comparison of our theoretical results with these experiments is further complicated by the fact that these are highly disparate block lengths, $Z_{PEO} \simeq 4Z_{PS}$, and so kinetic effects which usually dominate in polymer crystallization may still be significant. Even if the measurements at $T_C = 43$ °C are for an equilibrium sample, a detailed comparison requires an accurate value of the fold energy E_{fold}. Given these uncertainties, we consider the agreement between theory and experiment to be encouraging.

Earlier work by Skoulios et al.[1] and Franta et al.[2] can be used for a second, albeit indirect, comparison. In PEO-*block*-PS/solvent systems, they measured domain thicknesses as functions of block molecular weights, crystallization temperature, and solvent concentration. In one series of measurements, they determined the thickness of the PEO layer as a function of T_C for a copolymer with number average degrees of polymerization $Z_{PEO} \simeq 380$ and

$Z_{PS} \simeq 80$, in which the PS was swollen with 30% ethylbenzene.[2] They found $d_{PEO} \simeq 11$ nm for $T_C = -20$ °C, increasing to $d_{PEO} \simeq 19$ nm at $T_C = 42$ °C. Interpreting these data using the single-layer model, these results correspond to the number of folds per block decreasing from $n_f = 8$ at $T_C = -20$ °C to $n_f = 5$ at the higher temperature. In a related series of measurements done at $T_C = 25$ °C, it was found that when the solvent concentration was reduced, n_f decreased. On the basis of the two sets of measurements, we conclude that for pure PEO-*block*-PS at equilibrium, $n_f \leq 5$. In our model, we calculate $n_f = 2$.

We can obtain scaling relations which predict all of the calculated trends. Recognizing that the only significant variation in the free energy density comes from f_{fold} and f_{am}, we can approximate the d dependence of f for large α by

$$f(d) = \frac{\bar{\rho}_{0B}}{\rho_{0A}}\bar{\phi}_{CB}\frac{n_f}{Z_{CB}}\frac{E_{fold}}{k_BT} + \frac{\bar{\phi}_{CA}}{Z_{CA}}g_\gamma(\alpha) \quad (7.1)$$

In the region of equilibrium, α is large enough that $g_\gamma(\alpha)$ can be approximated by the first term

$$g_\gamma(\alpha) \simeq 0.016\alpha^\mu/\sqrt{\gamma} \quad (7.2)$$

The number of folds is $n_f = n - 1$, and the number of segments per molecule is

$$n = W\frac{Z_{CB}}{R}\frac{c}{d_B} \quad (7.3)$$

where R is the number of monomers per crystallographic length c ($R = 7$ for PEO) and $W = 1$ or 2 for the single- or double-layer models, respectively. For obtaining the scaling relations it is adequate to take $\tilde{d}_\kappa = d_\kappa$. Using $\bar{\phi}_K = \tilde{d}_\kappa/d = (Z_{C\kappa}\rho_{0C})/(Z_C\rho_{0\kappa})$, eq 7.1 becomes

$$f(d) \simeq \frac{\rho_{0C}}{\rho_{0A}Z_C}\left\{\left[\frac{W_c}{R}\frac{\rho_{0B}}{\rho_{0C}}\frac{Z_C}{d} - 1\right]\frac{E_{fold}}{k_BT} + 0.016(3^{\mu/2})\left(\frac{\rho_{0C}}{\rho_{0A}}\right)^\mu \frac{b_A^{(1/2)-\mu}}{\sqrt{a}}Z_{CA}^{(1+2\mu)/4}\left(\frac{d}{Z_C}\right)^\mu\right\} \quad (7.4)$$

Minimizing with respect to d and dropping numerical constants, we obtain for the crystalline segments

$$n_{eq} \propto W^{\mu/(1+\mu)}\left[\frac{\rho_{0B}}{\rho_{0A}}\right]^{\mu/(1+\mu)}\left[\frac{k_BT}{E_{fold}}\right]^{1/(1+\mu)}Z_{CA}^{\upsilon} \quad (7.5)$$

and for the amorphous blocks

$$\alpha_{eq} \propto W^{1/(1+\mu)}\left[\frac{\rho_{0B}}{\rho_{0A}}\right]^{1/(1+\mu)}\left[\frac{E_{fold}}{k_BT}\right]^{1/(1+\mu)}Z_{CA}^{w} \quad (7.6)$$

and for the overall repeat distance

$$d_{eq} \propto W^{1/(1+\mu)}\frac{[\rho_{0B}\rho_{0A}{}^\mu]^{1/(1+\mu)}}{\rho_{0C}}\left[\frac{E_{fold}}{k_BT}\right]^{1/(1+\mu)}\frac{Z_C}{Z_{CA}{}^\upsilon} \quad (7.7)$$

In these results, $\upsilon = (1 + 2\mu)/[4(1 + \mu)]$ and $w = {}^1/_2 - \upsilon$. Both ρ_{0B} and ρ_{0A} are constant, and ρ_{0C} depends only slowly on the ratio Z_{CA}/Z_{CB}. Neglecting this dependence and taking $\mu = 2$, we thus have

$$n_{eq} \propto W^{2/3}\left[\frac{k_BT}{E_{fold}}\right]^{1/3}Z_{CA}{}^{5/12} \quad (7.8)$$

$$\alpha_{eq} \propto W^{1/3}\left[\frac{E_{fold}}{k_BT}\right]^{1/3}Z_{CA}{}^{1/12} \quad (7.9)$$

$$d_{eq} \propto W^{1/3}\left[\frac{E_{fold}}{k_BT}\right]^{1/3}Z_CZ_{CA}{}^{-5/12} \quad (7.10)$$

Combining these with eq 3.17 and 7.3, the individual layer thicknesses scale with degrees of polymerization as $d_B \propto Z_{CB}Z_{CA}{}^{-5/12}$ and $d_A \propto Z_{CA}{}^{7/12}$.

These simple results are in good agreement with the full calculations. First, we note that the scaling is the same for the single- and double-layer models. Next we see explicitly that both n_{eq} and α_{eq} are independent of Z_{CB} and scale as $Z_{CA}{}^{5/12}$ and $Z_{CA}{}^{1/12}$, respectively. These exponents are related as follows. If the number of segments, n, were independent of Z_{CA}, then d_A would scale linearly with Z_{CA} to maintain constant density and α_{eq} would correspondingly scale as $Z_{CA}{}^{1/12}$. However, since $n_{eq} \propto Z_{CA}{}^\upsilon$ (eq 7.5), the change in folding gives $\alpha_{eq} \propto Z_{CA}{}^{(1/2)\upsilon}$. Thus, the variation in folding almost entirely compensates for the variation of α_{eq} with Z_{CA} at equilibrium. Finally, the equilibrium layer thickness d scales as $Z_CZ_{CA}{}^{-5/12}$. For $Z_{CA} \ll Z_{CB}$ this tends to $Z_{CB}Z_{CA}{}^{-5/12}$, increasing with increasing Z_{CB} but decreasing with increasing Z_{CA}. For $Z_{CA} \gg Z_{CB}$, it tends to $Z_{CA}{}^{7/12}$, independent of Z_{CB}, but increasing with increasing Z_{CA}. Although these extreme limits are not reached in our calculations and presumably would not occur in real systems because of competing morphologies, the cross-over behavior evident in Figure 13 is in agreement with these trends. Finally, note that all these results scale approximately as $[E_{fold}/k_BT]^{\pm 1/3}$.

The differences between the single- and double-layer models appear in the prefactor. Compared with the single-layer model, for the double-layer model n_{eq} and α_{eq} are predicted to be larger by factors of $2^{2/3} \simeq 1.6$ and $2^{1/3} \simeq 1.25$, consistent with our numerical work. The total repeat distance is also larger by a factor of about 1.25.

Finally, note that eq 7.3–7.10 apply to any crystallizable diblock copolymers; thus, we predict the same scaling laws and general behavior for all such materials. This is consistent with the experimental results of Gervais et al.[4-11] Their results for PCL-*block*-PS were similar to those for PEO-*block*-PS, except that the influence of the PS block on n_f was reduced. This reduction may be due to nonequilibrium effects.

8. Conclusions

We have presented a theory of the equilibrium morphology of diblock copolymers in which one block is crystallizable and the other amorphous. The amorphous blocks are modelled as flexible chains, which we describe by a mean field self-consistent theory of the polymer distribution functions. The crystallizable block is modelled as a semicrystalline, folded chain, lamellar structure. The chemical bonds joining the blocks are localized in interphases between the amorphous and crystalline regions.

The expression for the free energy can be interpreted as a sum of four main contributions: the free energy of the amorphous block, that of the crystalline block, the interaction energy of the two blocks, and the reduced entropy due to the localization of the copolymer joints to the interphases. The first two are the significant factors that control the equilibrium lamellar thickness.

The free energy of the amorphous block can be expressed as a universal function, g, of two arguments, one specifying the thickness of the amorphous region relative to the size of unstretched molecule and the other specifying the relative thickness of the interphase. As the spacing increases, this energy increases due to the increased stretching. For a given stretching, the free energy is higher for a narrow interphase.

The crystalline free energy is characterized by the heat of fusion and the fold energy. For a given molecular weight, as the lamellae thicken, the crystalline blocks unfold, thus reducing the free energy. We have calculated

equilibrium morphologies for a variety of relative molecular weights for the specific case PEO-*block*-PS. The results can be summarized by focussing on the number of segments, n_{eq}, in each crystalline block and the stretching of the amorphous block, α_{eq}, which depend on the degree of polymerization of the amorphous block but are independent of the degree of polymerization of the crystalline block. Both these quantities increase as the cube root of the fold energy. These results are summarized by eq 7.8 and 7.9. The equilibrium repeat distance, d, depends on the degrees of polymerization of both blocks. This is summarized by eq 7.10. A slight equilibrium temperature dependence is also predicted for all these quantities.

There is very little experimental data available for comparison with theory. We end with an appeal for equilibrium measurements on these types of systems, as well as accurate determinations of the fold energies for the crystalline blocks.

Acknowledgment. We thank L. Marks for developing the mathematical techniques and computer programs for solving the self-consistent diffusion equations. M.D.W. thanks the Natural Sciences and Engineering Research Council of Canada for the award of a Senior Industrial Fellowship and the Xerox Research Centre of Canada for their hospitality during the course of much of this work.

Appendix A. General Theory of Multicomponent Systems

The starting point of the general theory is an expression for the partition function of a system of copolymers, homopolymers and solvent molecules, which can be written as[13]

$$\mathbf{Z} = \left(\prod_{\kappa}^{C} \frac{z_\kappa^{\tilde{N}_\kappa}}{\tilde{N}_\kappa!}\right) \times \int \left(\prod_{s}\prod_{i=1}^{\tilde{N}_s} d^3r_{si}\right)\left(\prod_{p}\prod_{j=1}^{\tilde{N}_p} \delta\mathbf{r}_{pj}(\cdot)P[\mathbf{r}_{pj}(\cdot)]\right) \times \int \left(\prod_{C}\prod_{r=1}^{\tilde{N}_C} \delta\mathbf{r}_{CAr}(\cdot)P[\mathbf{r}_{CAr}(\cdot)]\right)\left(\prod_{C}\prod_{t=1}^{\tilde{N}_C} \delta\mathbf{r}_{CBt}(\cdot)\tilde{P}[\mathbf{r}_{CBt}(\cdot)]\right) \times \int \left\{\prod_{C}\prod_{r=1}^{\tilde{N}_C} \delta[\mathbf{r}_{CAr}(Z_{CA}) - \mathbf{r}_{CBr}(Z_{CB})]\right\} \times e^{-\beta V} \quad (A.1)$$

In our notation κ denotes any type of component, s solvent, p homopolymer, and C copolymer. There are $\tilde{N}_s$ solvent molecules of type s and $\tilde{N}_p$ and $\tilde{N}_C$ homopolymers and copolymers of types p and C, respectively. The degrees of polymerization of homopolymers are denoted Z_p and $N_p = \tilde{N}_p Z_p$ is the total number of monomers of type p. The degree of polymerization of the copolymers is $Z_C = Z_{CB} + Z_{CA}$, where Z_{CB} and Z_{CA} refer to the B and A blocks. Different components (e.g., different types of homopolymers) could refer to differences in chemical species, molecular weight, tacticity, etc.

In eq A.1, z_κ is the partition function due to the kinetic energy of a molecule of type κ. The C over the product sign indicates that for that product the copolymer is to be treated as a single component. The integrals are over all space curves $\mathbf{r}(\cdot)$ which represent possible configurations of the macromolecules. The homopolymers and the amorphous blocks of the copolymers are modelled as flexible chains. The corresponding probability density functional for a given space curve is assumed to be of the standard Wiener form

$$P[\mathbf{r}_\kappa(\cdot)] \propto \exp\left[-\frac{3}{2b_\kappa^2}\int_0^{Z_\kappa} dt\ \dot{\mathbf{r}}_\kappa^2(t)\right] \quad (A.2)$$

for κ = p, CA, with b_κ the Kuhn statistical length of a single segment of the polymers. This function describes the intramolecular bonding. For the crystallizable blocks (CB) these interactions will be included in the heat of fusion and fold energy so that $\tilde{P}[\mathbf{r}_{CB}(\cdot)]$ does not need to be specified in this case. The Dirac delta functions ensure that one end of each of the two blocks of each copolymer occupy the same points in space, i.e., that they are bonded together at the joint.

The microscopic particle densities can be expressed as

$$\hat{\rho}_s(\mathbf{r}) = \sum_{i=1}^{\tilde{N}_s} \delta(\mathbf{r} - \mathbf{r}_{si}) \quad (A.3)$$

$$\hat{\rho}_P(\mathbf{r}) = \sum_{J=1}^{\tilde{N}_P} \int_0^{Z_P} dt\ \delta(\mathbf{r} - \mathbf{r}_{PJ}(t)) \quad (A.4)$$

where P and J refer to either homopolymer or a block of the copolymer. Using these and defining $\hat{W} = \beta V$ with $k_B T = 1/\beta$ as the unit of energy, the intermolecular potential can be written

$$\hat{W} = \tfrac{1}{2}\sum_{\kappa\kappa'} \int d^3r \int d^3r'\ \hat{\rho}_\kappa(\mathbf{r}) W_{\kappa\kappa'}(\mathbf{r} - \mathbf{r}')\hat{\rho}_{\kappa'}(\mathbf{r}') \quad (A.5)$$

Introducing the δ function, we have

$$e^{-\hat{W}} = \int \left(\prod_\kappa \delta\rho_\kappa(\cdot)\right)\left[\prod_\kappa \delta(\rho_\kappa(\cdot) - \hat{\rho}_\kappa(\cdot))\right] e^{-W} \quad (A.6)$$

where W is defined as in eq A.5 but with $\hat{\rho}_\kappa(\cdot)$ replaced by $\rho_\kappa(\cdot)$. Using an integral representation of the δ function

$$\delta[\rho_\kappa(\cdot) - \hat{\rho}_\kappa(\cdot)] = \mathcal{N}\int \delta\omega_\kappa(\cdot)\ \exp\left\{\int d^3r\ \omega_\kappa(\mathbf{r})[\rho_\kappa(\mathbf{r}) - \hat{\rho}_\kappa(\mathbf{r})]\right\} \quad (A.7)$$

where the limits on the integral over ω_κ are $\pm i\infty$ and $\mathcal{N}$ is a normalization constant, the partition function becomes

$$\mathbf{Z} = \left(\prod_\kappa^C \frac{z_\kappa^{\tilde{N}_\kappa}}{\tilde{N}_\kappa!}\right)\int \left[\prod_\kappa \delta\rho_\kappa(\cdot)\delta\omega_\kappa(\cdot)\right] \times \left(\prod_\kappa^C \mathbf{Q}_\kappa^{\tilde{N}_\kappa}\right) \exp\left[\sum_\kappa \int d^3r\ \omega_\kappa(\mathbf{r})\rho_\kappa(\mathbf{r}) - W\right] \quad (A.8)$$

with

$$\mathbf{Q}_s = \int d^3d\ e^{-\omega_s(\mathbf{r})} \quad (A.9)$$

$$\mathbf{Q}_p = \int \delta\mathbf{r}(\cdot)\ P[\mathbf{r}_p(\cdot)]\ \exp\left\{-\int_0^{Z_p} dt\ \omega_p[\mathbf{r}(t)]\right\} \quad (A.10)$$

$$\mathbf{Q}_C = \int \delta\mathbf{r}_{CA}(\cdot)\ P[\mathbf{r}_{CA}(\cdot)]\ \exp\left\{-\int_0^{Z_{CA}} dt\ \omega_{CA}[\mathbf{r}_{CA}(t)]\right\} \times \delta\mathbf{r}_{CB}(\cdot)\tilde{P}[\mathbf{r}_{CB}(\cdot)]\ \exp\left\{-\int_0^{Z_{CB}} dt\ \omega_{CB}[\mathbf{r}_{CB}(t)]\right\} \times \delta[\mathbf{r}_{CA}(Z_{CA}) - \mathbf{r}_{CB}(Z_{CB})] \quad (A.11)$$

Equation A.8 is formally the same as the expression derived earlier for amorphous copolymers. Equations A.9 and A.10 are also the same. However, the expression for $\mathbf{Q}_C$ differs from the earlier result by the fact that one copolymer block is crystallizable, formally through the appearance of $\tilde{P}_{CB}$.

As before, $\mathbf{Q}_p$ can be written

$$\mathbf{Q}_p = \int d^3r\ d^3r_0\ Q_p(\mathbf{r}, Z_p|\mathbf{r}_0) \quad (A.12)$$

where $Q_p(\mathbf{r},t|\mathbf{r}_0)$ satisfies[14]

$$\frac{\partial}{\partial t}Q_p = \left(\frac{b_p^2}{6}\nabla^2 - \omega_p\right)Q_p \quad (A.13)$$

with the initial condition

$$Q_p(\mathbf{r},0|\mathbf{r}_0) = \delta(\mathbf{r} - \mathbf{r}_0) \tag{A.14}$$

except for those regions (values of $\mathbf{r}$) where $Q_p(\mathbf{r},t|\mathbf{r}_0) = 0$. Or, if we introduce

$$q_p(\mathbf{r},t) = \int d^3r_0\, Q_p(\mathbf{r},t|\mathbf{r}_0) \tag{A.15}$$

then q_p satisfies the same differential equation but is subject to the initial condition

$$q_p(\mathbf{r},0) = 1 \tag{A.16}$$

except where $q_p(\mathbf{r},t) = 0$.

We also have

$$\mathbf{Q}_p = \int d^3r\, q_p(\mathbf{r},Z_p) \tag{A.17}$$

As usual, $Q_p(\mathbf{r},t|\mathbf{r}_0)$ can be interpreted as the unnormalized probability distribution function for a chain of t repeat units which starts at $\mathbf{r}_0$ and ends at $\mathbf{r}$; q_p is proportional to the probability that the chain ends at $\mathbf{r}$, independent of its starting point.

For the copolymers, we can write

$$\mathbf{Q}_C = \int d^3r\, d^3r_0\, d^3r_1\, d^3r_2\, Q_{CA}(\mathbf{r},Z_{CA}|\mathbf{r}_0)\delta(\mathbf{r} - \mathbf{r}_1)\tilde{Q}_{CB}(\mathbf{r}_1,Z_{CB}|\mathbf{r}_2)$$

$$\mathbf{Q}_C = \int d^3r_1\, q_{CA}(\mathbf{r}_1,Z_{CA})\tilde{q}_{CB}(\mathbf{r}_1,Z_{CB}) \tag{A.18}$$

with q_{CA} and $\tilde{q}_{CB}$ defined by

$$q_{CA}(\mathbf{r}_1,Z_{CA}) = \int d^3\mathbf{r}_0\, Q_{CA}(\mathbf{r}_1,Z_{CA}|\mathbf{r}_0) \tag{A.19}$$

$$\tilde{q}_{CB}(\mathbf{r}_1,Z_{CB}) = \int d^3\mathbf{r}_2\, \tilde{Q}_{CB}(\mathbf{r}_1,Z_{CB}|\mathbf{r}_2) \tag{A.20}$$

The functions Q_{CA} and q_{CA} satisfy the same kind of modified diffusion equations[14] (with the appropriate ω_κ and Z_κ) as Q_p and q_p. Physically, this is because they describe amorphous polymer blocks within the same approximations used for the homopolymers. $\tilde{Q}_{CB}$ and $\tilde{q}_{CB}$, describing the crystallizable blocks, are not given by the solution of a diffusion equation. However, from eq A.12, we see that they are related to inter- and intramolecular potentials in the same way as Q_{CA} and q_{CA}. Hence, $\tilde{q}_{CB}(\mathbf{r},Z_{CB})$ is proportional to the probability that the CB block ends at $\mathbf{r}$. We will use this below.

Using Stirling's expansion for large $\tilde{N}_\kappa$ we can write the partition function (eq A.8) as

$$\mathbf{Z} = \mathcal{N} \int \left(\prod_\kappa \delta\rho_\kappa(\cdot)\delta\omega_\kappa(\cdot)\right) \exp[-F(\{\rho_\kappa(\cdot)\},\{\omega_\kappa(\cdot)\})] \tag{A.21}$$

where the free energy functional in units of k_BT is given by

$$F(\{\rho_\kappa(\cdot)\},\{\omega_\kappa(\cdot)\}) = \left[W(\{\rho_\kappa(\cdot)\}) - \sum_\kappa \int d^3r\, \omega_\kappa(\mathbf{r})\rho_\kappa(\mathbf{r})\right] + \sum_\kappa^C \tilde{N}_\kappa \left\{\ln \frac{\tilde{N}_\kappa}{z_\kappa \mathbf{Q}_\kappa} - 1\right\} \tag{A.22}$$

The integral of eq A.21 can be evaluated by the saddle-point method. We thereby obtain the free energy by minimizing the functional (eq A.22) subject to the constraint of a constant number of particles

$$\int d^3r\, \rho_\kappa(\mathbf{r}) = N_\kappa \tag{A.23}$$

and no volume change locally upon mixing

$$\sum_\kappa \phi_\kappa(\mathbf{r}) = 1 \tag{A.24}$$

where $\phi_\kappa(\mathbf{r})$ is the local volume fraction of component κ defined by

$$\phi_\kappa(\mathbf{r}) = \rho_\kappa(\mathbf{r})/\rho_{0\kappa} \tag{A.25}$$

and $\rho_{0\kappa}$ is the density of pure material in monomer segments per unit volume. We introduce Lagrange multipliers $-\lambda_\kappa$ and $\eta(\mathbf{r})$ corresponding to eq A.23 and A.24, respectively. Minimizing with respect to the ρ_κ gives

$$\frac{\delta W}{\delta\rho_\kappa(\mathbf{r})} - \omega_\kappa(\mathbf{r}) + \frac{\eta(\mathbf{r})}{\rho_{0\kappa}} - \lambda_\kappa = 0 \tag{A.26}$$

for all components. Minimizing with respect to the ω_κ gives

$$\rho_\kappa(\mathbf{r}) + \frac{\tilde{N}_\kappa}{\mathbf{Q}_\kappa}\frac{\delta\mathbf{Q}_\kappa}{\delta\omega_\kappa(\mathbf{r})} = 0 \tag{A.27}$$

for the solvent and homopolymer (κ = s, p) and

$$\rho_{C\kappa}(\mathbf{r}) + \frac{\tilde{N}_C}{\mathbf{Q}_C}\frac{\delta\mathbf{Q}_C}{\delta\omega_{C\kappa}(\mathbf{r})} = 0 \tag{A.28}$$

for the blocks of copolymer (Cκ = CA, CB).

Combined with eq A.9 and A.10, eq A.27 gives

$$\rho_s(\mathbf{r}) = (N_s/\mathbf{Q}_s)e^{-\omega_s(\mathbf{r})} \tag{A.29}$$

and

$$\rho_p(\mathbf{r}) = \frac{\tilde{N}_p}{\mathbf{Q}_p}\int_0^{Z_p} dt\, q_p(\mathbf{r},t)q_p(\mathbf{r},Z_p - t) \tag{A.30}$$

for solvent and homopolymer. For the A block of the copolymer

$$\rho_{CA}(\mathbf{r}) = \frac{\tilde{N}_C}{\mathbf{Q}_C}\int_0^{Z_{CA}} dt\, q_{CA}(\mathbf{r},t)\int d^3r_0\, Q_{CA}(\mathbf{r},Z_{CA} - t|\mathbf{r}_0)\tilde{q}_{CB}(\mathbf{r}_0,Z_{CB}) \tag{A.31}$$

This is the same as eq 4.3 of Hong and Noolandi,[13] except that $\tilde{q}_{CB}$ describes crystallizable blocks and $\mathbf{Q}_C$ is correspondingly modified. We do not need an expression for ρ_{CB} analogous to eq A.31 in this paper.

Expressions for the self-consistent potentials for the amorphous polymers are obtained from (A.5) and (A.26) as shown earlier.[13] For a short-range potential, a gradient expansion of W gives

$$W = \tfrac{1}{2}\sum_\kappa W_{\kappa\kappa}\rho_{0\kappa}N_\kappa + \tfrac{1}{2}\sum_{\kappa\kappa'} U_{\kappa\kappa'}\int d^3r\, \rho_\kappa(\mathbf{r})\rho_{\kappa'}(\mathbf{r}) - \tfrac{1}{12}\sum_{\kappa\kappa'} V_{\kappa\kappa'}\int d^3r\, \nabla\rho_\kappa(\mathbf{r})\cdot\nabla\rho_{\kappa'}(\mathbf{r}) + \ldots \tag{A.32}$$

Detailed expressions for $W_{\kappa\kappa'}$, $U_{\kappa\kappa'}$, and $V_{\kappa\kappa'}$ are given in ref 13. At this point, we note that $V_{\kappa\kappa'} = \sigma^2_{\kappa\kappa'}U_{\kappa\kappa'}$, where $\sigma_{\kappa\kappa'}$, is the range of the potential. Using (A.32) in (A.26) gives

$$\omega_\kappa(\mathbf{r}) = \omega_\kappa(\mathbf{r}^b) + \frac{\eta(\mathbf{r}) - \eta(\mathbf{r}^b)}{\rho_{0\kappa}} + \sum_{\kappa'} U_{\kappa\kappa'}\left[\rho_{\kappa'}(\mathbf{r}) - \rho_{\kappa'}(\mathbf{r}^b) + \frac{\sigma^2_{\kappa\kappa'}}{6}(\nabla^2\rho_{\kappa'}(\mathbf{r}) - \nabla^2\rho_{\kappa'}(\mathbf{r}^b))\right] \tag{A.33}$$

Here $\mathbf{r}^b$ is any reference point and $\omega_\kappa(\mathbf{r}^b)$ is the value of the potential at that point. Both of these can be chosen for convenience.

To fully specify $\omega_\kappa(\mathbf{r})$, we need to eliminate the Lagrange multiplier. If we are dealing with a system in which solvent is present, then from eq A.29

$$\omega_s(\mathbf{r}) - \omega_s(\mathbf{r}^b) = \ln \rho_s(\mathbf{r}^b)/\rho_s(\mathbf{r}) \tag{A.34}$$

This can be substituted into eq A.33 to derive an explicit expression for $\eta(\mathbf{r}) - \eta(\mathbf{r}^b)$, which can then be used to obtain an expression for $\omega_\kappa(\mathbf{r})$ for each component, in terms

of the density distributions of all components $\{\rho_\kappa(\mathbf{r})\}$. In the case of the pure copolymer, there is no expression for the solvent concentration to which η can be related. This case is treated in detail in section 2.

It is convenient to evaluate the free energy F relative to that of a reference state of a hypothetical uniform melt in which the density of each component is given by

$$\bar{\rho}_\kappa = \rho_{0\kappa}\bar{\phi}_\kappa \tag{A.35}$$

$\bar{\phi}_\kappa$ is the overall macroscopic volume fraction of component κ and $\rho_{0\kappa}$ is the density of the pure component. Denoting the free energy of this by F^{ref}, we focus on

$$\Delta F = F - F^{\text{ref}} \tag{A.36}$$

where, using eq A.22

$$F^{\text{ref}} = W(\{\bar{\rho}_\kappa\}) - \sum_\kappa \int \mathrm{d}^3r\, \bar{\omega}_\kappa\bar{\rho}_\kappa + \sum_\kappa^{\mathrm{C}} \tilde{N}_\kappa \left\{ \ln \frac{\tilde{N}_\kappa}{z_\kappa \bar{\mathbf{Q}}_\kappa} - 1 \right\} \tag{A.37}$$

and $\bar{\omega}_\kappa$ and $\bar{\mathbf{Q}}_\kappa$ (and $\bar{\rho}_\kappa$) all refer to the reference state. Simplifying this, we note first

$$W(\{\bar{\rho}_\kappa\}) = \tfrac{1}{2}\sum_\kappa W_{\kappa\kappa}\rho_{0\kappa}N_\kappa + \tfrac{1}{2}\sum_{\kappa\kappa'} U_{\kappa\kappa'} \int \mathrm{d}^3r\, \bar{\rho}_\kappa\bar{\rho}_{\kappa'} \tag{A.38}$$

For the solvent, we have

$$\bar{\rho}_{\mathrm{s}} = (\tilde{N}_{\mathrm{s}}/\bar{\mathbf{Q}}_{\mathrm{s}})e^{-\bar{\omega}_{\mathrm{s}}} \tag{A.39}$$

and for homopolymers, since $\bar{q}_{\mathrm{p}}(\mathbf{r},t)$ is uniform, we obtain from the "steady-state" solution of the diffusion equation

$$\bar{q}_{\mathrm{p}}(\mathbf{r},t) = \bar{q}_{\mathrm{p}}(t)$$

$$\bar{q}_{\mathrm{p}}(\mathbf{r},t) = e^{-\bar{\omega}_{\mathrm{p}}t} \tag{A.40}$$

which is used in eq A.31 to give

$$\bar{\rho}_{\mathrm{p}} = \frac{\tilde{N}_{\mathrm{p}}}{\bar{Q}_{\mathrm{p}}} Z_{\mathrm{p}} e^{-\bar{\omega}_{\mathrm{p}}Z_{\mathrm{p}}} \tag{A.41}$$

Similarly, for the copolymer

$$\bar{q}_{\mathrm{CA}}(\mathbf{r},t) = e^{-\bar{\omega}_{\mathrm{CA}}t} \tag{A.42}$$

which when used in eq A.31 gives

$$\bar{\rho}_{\mathrm{CA}} = \frac{\tilde{N}_{\mathrm{C}}}{\bar{\mathbf{Q}}_{\mathrm{C}}} Z_{\mathrm{CA}} e^{-\bar{\omega}_{\mathrm{CA}}Z_{\mathrm{CA}}} \tilde{\bar{q}}_{\mathrm{CB}}(Z_{\mathrm{CB}}) \tag{A.43}$$

Using eq A.42 in eq A.18 yields

$$\bar{Q}_{\mathrm{C}} = e^{-\bar{\omega}_{\mathrm{CA}}Z_{\mathrm{CA}}} \tilde{\bar{q}}_{\mathrm{CB}}(Z_{\mathrm{CB}})V \tag{A.44}$$

where V is the total volume of the system. Finally, with these results, eq A.37 simplifies to

$$F^{\text{ref}} = W(\{\rho_\kappa\}) + \sum_\kappa^{\mathrm{C}} \tilde{N}_\kappa \left\{ \ln \frac{\bar{\rho}_\kappa}{z_\kappa Z_\kappa} - 1 \right\} + \sum_{\mathrm{C}} \tilde{N}_{\mathrm{C}} \ln \frac{e^{-\bar{\omega}_{\mathrm{CB}}Z_{\mathrm{CB}}}}{\tilde{\bar{q}}_{\mathrm{CB}}(Z_{\mathrm{CB}})} \tag{A.45}$$

where for the copolymers $\bar{\rho}_{\mathrm{C}} = \tilde{N}_{\mathrm{C}}Z_{\mathrm{C}}/V$.

The last sum, done over only copolymers, is due to the crystallizable blocks. Using the above result, along with eq A.22 and A.36, we arrive at our expression for ΔF, given as eq 2.1 of the main text.

Appendix B. Self-Consistent Solution of Diffusion Equation

The self-consistent solution requires solving the partial differential equations for $q(x,t)$, $q_1(x,t)$, and $q_2(x,t)$ and finding the mean field potential $\omega(x)$ so that the volume fraction $\phi(x)$ takes a prescribed (target) value $\phi^t(x)$ on the interval $[0,d_{\mathrm{A}}]$. (For simplicity, we drop the subscripts "CA" in the appendices.)

The equations are scaled so that $x \in [0,d_{\mathrm{A}}]$ is mapped onto $y \in [0,\pi]$ and $t \in [0,Z]$ is mapped onto $t' \in [0,1]$. The distributio functions then satisfy [$\psi = q$, q_1, or q_2)

$$\frac{1}{T}\frac{\partial}{\partial t'}\psi = \left(\frac{\partial^2}{\partial y^2} - \omega^*\right)\psi \tag{B.1}$$

where

$$T = \frac{Z\pi^2 b_{\mathrm{A}}{}^2}{6 d_{\mathrm{A}}{}^2} \tag{B.2}$$

and

$$\omega^*(y) = (Z/T)\omega(x) \tag{B.3}$$

The initial conditions are

$$q(y,0) = 1$$

$$q_1(y,0) = \theta\left(\frac{a\pi}{d_{\mathrm{A}}} - y\right) \tag{B.4}$$

$$q_2(y,0) = \theta\left[y - \pi\left(1 - \frac{a}{d_{\mathrm{A}}}\right)\right]$$

with the boundary conditions

$$\psi(0,t') = \psi(\pi,t') = 0 \tag{B.5}$$

The convolutions are then appropriate modified; for example eq 3.9 becomes

$$\phi_\mu(x) = \bar{\phi}\frac{d}{a}\frac{\int_0^1 \mathrm{d}t'\, q(x,t')q_\mu(x,1-t')}{2\langle q(1)\rangle_a} \tag{B.6}$$

On the interval $[0,\pi]$, ω^* is symmetric, and $\omega^*(y) = \omega^*(\pi - y)$, and on the interval $[0,\pi/2]$ it is univalent, rising monotonically from a finite value to a single maximum $\omega_m{}^*$ at $y_{m'}$ and then decreasing to its value at $y = \pi/2$, which we take as zero for reference. In the subintervals $[0,y_m]$ and $[y_m,\pi/2]$, ω^* is approximated by the test monotonic functions

$$c_i y^{f_i(1-y)^{g_i}} + d_i \tag{B.7}$$

where $i = 1$ or 2 (for the two subintervals). This description of ω^* incorporates seven positive variables, y_m, $\omega_m{}^*$, $\omega^*(0)$, f_1, g_1, f_2, and g_2.

For a particular ω^*, the differential equations are solved via the eigenfunction expansions

$$q(y,t) = \sum_n a_n e^{-\lambda_n t} f_n(y)$$

$$q_1(y,t) = \sum_n b_n e^{-\lambda_n t} f_n(y) \tag{B.8}$$

$$q_2(y,t) = \sum_n c_n e^{-\lambda_n t} f_n(y)$$

where the f_n and λ_n are the eigensolutions of

$$\left(-\frac{\partial^2}{\partial y^2} + \omega^*(y)\right) f_n(y) = \lambda_n f_n(y) \tag{B.9}$$

and the expansion coefficients are determined from the initial conditions.

The eigenvalue problem is solved by approximating ω^* by a stepwise constant function with equal numbers of steps in the two subintervals. In each interval f_n is a linear combination of analytic circular or hyperbolic functions,

with coefficients chosen so that f_n is everywhere continuous with continuous derivatives.

In constructing the $\phi(x)$ (eq 3.8), $\phi_1(x)$, and $\phi_2(x)$ can be combined, with the result that only the symmetric eigenfunctions are needed. Depending on the amount to which the polymer is stretched, i.e., the value of α as defined by eq 3.17, anywhere from 20 to 1000 eigenfunctions are needed. In order to calculate individually the contributions ϕ_1 and ϕ_2, as in Figures 5 and 6, both even and odd eigenfunctions are needed, i.e., up to 2000 in total.

The object of the calculation is to find the ω^* which produces the predetermined $\phi^t(x)$. This is done by minimizing the error

$$\epsilon = \sum_n [\phi(y_n) - \phi^t(y_n)]^2 \tag{B.10}$$

with respect to the seven parameters of the potential using the simplex algorithm. Typically we were able to obtain $\epsilon < 0.005$, providing three or four significant figures in the free energy. We found that the largest values of α for which we were able to find solutions were about seven or eight, depending on γ. Beyond this, the best solutions achievable had oscillations in the calculated $\phi(y)$. We terminated the calculations at values of α such that the error ϵ (as defined above) exceeds about 0.02. Figure 6 illustrates these effects for $\gamma = 0.05$. In the bottom panel, for which $\alpha = 6$, the error is not quite 0.01. As seen in Figure 7, we calculated the free energy out to $\alpha = 6.4$ in this case. On the other hand, our process, coupled with the functional form of potential of expression eq B.7, suppresses spurious oscillations in the potential such as those encountered by Helfand.[14]

Appendix C. Functional Dependence of the Free Energy for the Amorphous Region

In this section, we derive eq 3.16 for f_{am}.

As discussed in Appendix B, we can map any interval $x \in [0,d_A]$ onto $y \in [0,\pi]$ and $t \in [0,Z]$ onto $t' \in [0,1]$. The partial differential equation is governed by the parameter T given by

$$T = \pi^2/2\alpha^2 \tag{C.1}$$

where α is the stretching parameter defined by eq 3.17. The initial conditions are specified in terms of the ratio a/d_A which can be expressed as

$$a/d_A = (3)^{1/2}(\gamma/\alpha) \tag{C.2}$$

where γ is the surface parameter of eq 3.18. In constructing the volume fractions, using $\bar{\phi}^a = (d/d_A)\,\bar{\phi}$ and eq B.6, we have

$$\phi_\mu(x) = \frac{a}{3^{1/2}\gamma} \frac{\int_0^1 dt'\, q(x,t')q_\mu(x,1-t')}{2\langle q_\mu(1)\rangle} \tag{C.3}$$

We have thus reformulated the self-consistent problem in terms of the two parameters α and γ. Turning now to eq 3.15, if we again map the interval $[0,d_A]$ onto $[0,\pi]$, we recover eq 3.16 with

$$g_\gamma(\alpha) = -\ln \langle q_{CA}(1)\rangle_a - \frac{\pi}{\bar{\phi}^a}\int_0^\pi dy\, \omega^*(y)\phi(y) \tag{C.4}$$

which is a function of only α and γ.

Registry No. (EO)(S) (block copolymer), 107311-90-0.

References and Notes

(1) Skoulios, A. E.; Tsouladze, G.; Franta, E. *J. Polym. Sci., Part C* **1963**, *4*, 507.
(2) Franta, E.; Skoulios, A. E.; Rempp, P.; Benoit, H. *Makromol. Chem.* **1965**, *87*, 271.
(3) (a) Lotz, B.; Kovacs, A. J. *Polym. Prepr. (Am. Chem. Soc., Div. Polym. Chem.)* **1969**, *10*(2), 820. (b) Lotz, B., private communication.
(4) Gervais, M.; Gallot, B. *Makromol. Chem.* **1973**, *171*, 157.
(5) Gervais, M.; Gallot, B. *Makromol. Chem.* **1973**, *174*, 193.
(6) Gervais, M.; Gallot, B. *Makromol. Chem.* **1977**, *178*, 1577.
(7) Gervais, M.; Gallot, B. *Makromol. Chem.* **1977**, *178*, 2071.
(8) Herman, J.-J.; Jérôme, R.; Teyssié, P.; Gervais, B.; Gallot, B. *Makromol. Chem.* **1978**, *179*, 1111.
(9) Gervais, M.; Gallot, B. *Makromol. Chem.* **1979**, *180*, 2041.
(10) Gervais, M.; Gallot, B. *Polymer* **1981**, *22*, 1129.
(11) Gervais, M.; Gallot, B.; Jérôme, R.; Teyssié, P. *Makromol. Chem.* **1981**, *182*, 989.
(12) DiMarzio, E. A.; Guttman, C. M.; Hoffman, J. D. *Macromolecules* **1980**, *13*, 1194.
(13) Hong, K. M.; Noolandi, J. *Macromolecules* **1981**, *14*, 727.
(14) Helfand, E.; Wasserman, Z. R. *Macromolecules* **1976**, *9*, 879.
(15) Semenov, A. N. *Sov. Phys–JETP (Engl. Transl.)* **1985**, *61*, 733.
(16) Ohta, T.; Kawasaki, K. *Macromolecules* **1986**, *19*, 2621.
(17) Hoffman, J. D.; Davis, G. T.; Lauritzen, J. I., Jr. In *Crystalline and Non-Crystalline Solids*; Hannay, N. B., Ed.; Plenum: New York, 1976; Vol. 3.
(18) Richardson, M. J.; Savill, N. G. *Polymer* **1977**, *18*, 3.
(19) Tadokoro, H.; Chatani, Y.; Yoshihara, T.; Tahara, S.; Murahasi, S. *Makromol. Chem.* **1964**, *73*, 109.